SIMULATIONS ON GLOW DISCHARGE: DEVELOPMENT AND VALIDATION OF ONE-DIMENSIONAL KINETIC MODEL BY PARTICLE IN CELL/MONTE CARLO COLLISION METHOD

A THESIS SUBMITTED TO
THE GRADUATE SCHOOL OF NATURAL AND APPLIED SCIENCES
OF
MIDDLE EAST TECHNICAL UNIVERSITY

BY

ÖZGECAN TİRYAKİ

IN PARTIAL FULFILLMENT OF THE REQUIREMENTS
FOR
THE DEGREE OF MASTER OF SCIENCE
IN
PHYSICS

AUGUST 2019

Approval of the thesis:

SIMULATIONS ON GLOW DISCHARGE: DEVELOPMENT AND VALIDATION OF ONE-DIMENSIONAL KINETIC MODEL BY PARTICLE IN CELL/MONTE CARLO COLLISION METHOD

submitted by **ÖZGECAN TİRYAKİ** in partial fulfillment of the requirements for the degree of **Master of Science in Physics Department, Middle East Technical University** by,

Prof. Dr. Halil Kalıpçılar
Dean, Graduate School of **Natural and Applied Sciences** _____

Prof. Dr. Altuğ Özpineci
Head of Department, **Physics** _____

Assoc. Prof. Dr. Serhat Çakır
Supervisor, **Physics, METU** _____

Examining Committee Members:

Prof. Dr. İsmail Rafatov
Physics, METU _____

Assoc. Prof. Dr. Serhat Çakır
Physics, METU _____

Assoc. Prof. Dr. Hüseyin Oymak
Physics, Atılım University _____

Date: 16.08.2019

I hereby declare that all information in this document has been obtained and presented in accordance with academic rules and ethical conduct. I also declare that, as required by these rules and conduct, I have fully cited and referenced all material and results that are not original to this work.

Name, Surname: Özgecan Tiryaki

Signature:

ABSTRACT

SIMULATIONS ON GLOW DISCHARGE: DEVELOPMENT AND VALIDATION OF ONE-DIMENSIONAL KINETIC MODEL BY PARTICLE IN CELL/MONTE CARLO COLLISION METHOD

Tiryaki, Özgecan
Master of Science, Physics
Supervisor: Assoc. Prof. Dr. Serhat Çakır

August 2019, 77 pages

Numerical codes for glow discharge plasma simulations were developed by using Particle in Cell/Monte Carlo Collision (PIC/MCC) method. The model is one-dimensional in coordinate space and three-dimensional in velocity space (1d3v). A modification of Direct Simulation Monte Carlo (DSMC) method known as null-collision method was used for particle collisions. MPI and sub-cycling were used for speed up. The code was validated using benchmarks for capacitively coupled helium discharges and tested with three-dimensional (3d3v) model of electron swarm in argon. Results of the code were compared with the presented results for radio frequency (RF) argon discharge. Code was further used to study effect of electron reflection at the boundaries for RF helium discharge.

Keywords: Gas Discharge, Plasma, Particle in Cell Method, Monte Carlo Collision Method

ÖZ

PARILTILI DEŞARJ ÜZERİNE SİMULASYONLAR: BİR BOYUTLU KİNETİK MODELİN HÜCREDE PARÇACIK/MONTE CARLO ÇARPIŞMA YÖNTEMİYLE GELİŞTİRİLMESİ VE DOĞRULANMASI

Tiryaki, Özgecan
Yüksek Lisans, Fizik
Tez Danışmanı: Doç. Dr. Serhat Çakır

Ağustos 2019, 77 sayfa

Parıltılı deşarj plazma simülayonları için nümerik kodlar, Hücrede Parçacık/Monte Carlo (PIC/MCC) çarpışma yöntemi kullanılarak geliştirilmiştir. Model koordinat uzayında bir boyutlu ve hız uzayında üç boyutludur (1d3v). Parçacık çarpışmalarında null-collision metodu olarak bilinen Doğrudan Simülasyon Monte Carlo (DSMC) metodunun bir modifikasyonu kullanılmıştır. Hızlanma için MPI ve sub-cycling kullanılmıştır. Kod, kapasitif olarak bağlanmış helyum deşarjları için kriterler kullanılarak doğrulandı ve argonda üç boyutlu (3d3v) elektron sürüsü modeli ile test edildi. Kodun sonuçları, radyo frekansı (RF) argon deşarjı için sunulan sonuçlarla karşılaştırıldı. Kod, RF Helyum deşarjı için sınırlardaki elektron yansımasının etkisini incelemek için de kullanılmıştır.

Anahtar Kelimeler: Gaz Deşarjı, Plazma, Hücrede Parçacık Yöntemi, Monte Carlo Çarpışma Yöntemi

To my family

ACKNOWLEDGEMENTS

I would like to express my gratitude to my supervisor Assoc. Prof. Dr. Serhat Çakır for his guidance and encouragements.

I would like to thank Prof. Dr. İsmail Rafatov for his invaluable advices and remarks.

I am very grateful and indebted to Emrah Erden. Without his help and support, this thesis would not have been possible.

I would also like to thank Dr. Cemre Kuşoğlu Sarıkaya for answering my questions and for giving me valuable information about particle simulations.

I want to thank TUBITAK ULAKBIM since the numerical calculations reported in this paper were performed at TUBITAK ULAKBIM, High Performance and Grid Computing Center (TRUBA resources).

TABLE OF CONTENTS

LIST OF TABLES

TABLES

LIST OF FIGURES

FIGURES

LIST OF SYMBOLS

SYMBOLS

α	Ionization coefficient [m^{-1}]
a	Acceleration [m s^{-2}]
v	Velocity [m s^{-1}]
N_0	Plasma density [m^{-3}]
N	Neutral density [m^{-3}]
γ	Secondary yield coefficient
r	Reflection coefficient
R	Uniform random number between (0,1)
μ	Mobility coefficient [m^2 V^{-1} s^{-1}]
D	Diffusion coefficient [m^2 s^{-1}]
J_j	Current density of particle type j [m^{-2} s^{-2} C]
n_j	Density of particle type j [m^{-3}]
χ	Scattering angle [rad]
η	Azimuth angle [rad]
θ,ϕ	Pre-collision velocity angles [rad]
σ	Collision cross section [m^{-2}]
ε_{rel}	Maximum relative error
q	Electric charge [C]

ρ	Charge density [C m^{-3}]
k	Boltzmann constant [1.38064852 x 10^{-23} $J\ K^{-1}$]
T_j	Temperature of particle type *j* [K]
V	Electric potential [V]
V_B	Breakdown voltage [V]
ε_0	Permittivity of free space [8.85418782 x 10^{-12} F m^{-1}]
L	Electrode distance [m]
Δt	Time step size [s]
t	Simulation time [s]
Δx	Grid size [m]
λ_D	Debye Length [m]
m	Mass of the particle [kg]
$f(\varepsilon)$	Electron energy distribution function
P	Collision probability
p	Pressure [Pa]
R_i	Ionization rate [m^{-3} s^{-1}]
ν	Collision frequency [s^{-1}]
ε	Energy of the particle [eV]
P_j	Heating rate of particle type *j* [W m^{-3}]

CHAPTER 1

INTRODUCTION

1.1. Motivation

Modeling of plasmas contributes wide range of applications and theory from industry to astrophysics. Gas discharges have immense use in microelectronics, integrated circuit production and other industries such as biomedical, automotive, aerospace, steel [1]. Sputtering, thin film deposition, etching, optical emission and mass spectroscopies are important processes for surface modification, optimization, detecting and analyzing chemical compositions. With developing technology and computational resources, more detailed and accurate modeling becomes possible. Simulations give insight about complex physics of discharges and plasmas that is not always possible to get with classical diagnostics or experiments and help development of more efficient technologies.

Main goal of this study is development and validation of one-dimensional kinetic model using particle-in-cell-Monte-Carlo (PIC-MCC) collision method. Validation and benchmarking are done with the available literature. Model is further used for investigating boundary effects of RF discharges.

1.2. Types of Plasmas

Conventional definition of fourth state of matter and name plasma goes back to the studies of Crookes and Langmuir on electrical discharges [2]. In general, plasma can be seen as collection of charged particles and neutrals. Classification is broad. Density and temperature of charged particles and ionization degree are to be considered. Ionization degree is given by the ratio $n_i/(n_i+n_g)$, here n_i and n_g are ion and neutral number densities. If this is in order of unity, plasma is fully ionized.

For weakly ionized plasmas, ratio is far below unity and for most of the cases they are far from thermal equilibrium as electron temperature is much greater than that of heavy ions. In this case, neutral density determining frequency of charged-neutral collisions becomes important parameter. For higher pressures, near or local thermal equilibrium could be reached as electron temperature reduces and becomes equal to the ion temperature. This is observed in transition from glow to arc regimes in direct current (DC) discharges.

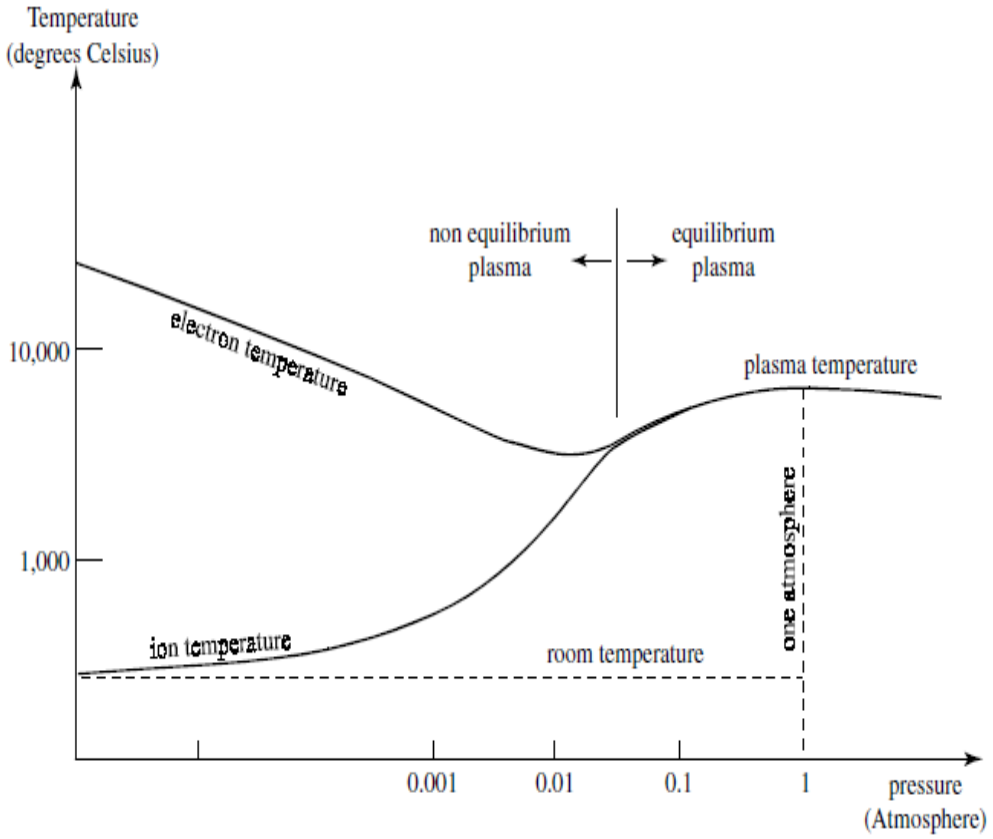

Figure 1.1. Pressure and temperature regimes for DC discharges [3].

In general, electron density is considered as plasma density and electron temperature are used to classify different types of plasmas.

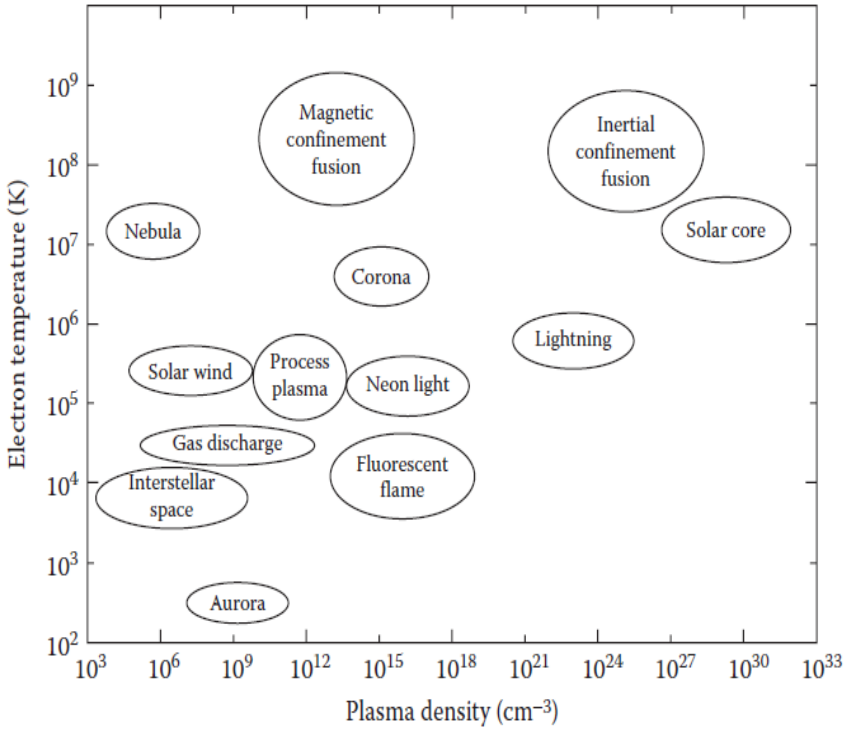

Figure 1.2. Plasma types for different electron temperature and density [4].

1.3. Modeling of Discharges

Numerical simulations help to understand different characteristics and properties of various types of discharges. There are mainly three types of modeling namely, kinetic or particle, fluid and hybrid methods. Particle method [5] uses so called macro or super particles that represent certain number of real particles to sample distribution function. Trajectories is followed by solving Lorentz equations of motion. Fluid method [6] solves first three velocity moments of Boltzmann equation, namely, density, momentum and energy conservation equations. Maxwell's equations are solved for electric and magnetic fields. Hybrid methods [7] combine kinetic and fluid methods. While kinetic method is used for one species, fluid method could be used for another depending on conditions. Main disadvantage of particle methods is numerical cost or computational time. However, they are accurate and reliable for

phenomena occurring in sheath region of discharges and at low pressure, non-thermal discharges where there is relatively small frequency of charged-neutral collisions. Advantage of fluid model is the application of more complex geometries relatively fast and it is reliable for thermal equilibrium regions. Hybrid method tries to combine advantages by using fluid method for slower species, while applying particle method to energetic ones [8]. Particle method is combined with the Monte-Carlo collision method to involve Coulomb or charged-neutral collisions.

CHAPTER 2

BASICS OF PLASMAS AND DISCHARGES

2.1. Breakdown and Townsend Discharge

There are number of ions and electrons in gasses on ambient conditions mostly due to external radiation. When an electric field is applied, current starts to increase as particles reaching electrodes. Loss of charges due to recombination limits the increase of the current. After further increase of the field, ionization rate increases and condition where all charged particles reach electrodes before recombination occurs. Current becomes independent of voltage and takes a saturation value. Saturation current density is limited by external sources [9] and given by

$$j = qd\frac{dn}{dt}, \tag{2.1}$$

where j is saturation current density, d is distance between electrodes, q is elementary charge and dn/dt is rate of production of the charged particles. Saturation current is very weak, discharge is very dark. After saturation, current increases again with voltage until the breakdown voltage is reached. Breakdown voltage depends on gas pressure, electrode spacing and material. Townsend discharge is the region between saturation and breakdown. In this region as electric field increases, ionization causes an electron avalanche and current increases above saturation value. Considering electron multiplication over a distance, current in the discharge can be written as

$$i = i_0 e^{\alpha d}, \tag{2.2}$$

where i_0 is the current at the cathode or primary current, α is first Townsend coefficient or ionization coefficient defined as number of ionization events made by

per electron, per unit distance. It depends strongly on ionization cross-section of electrons and pressure of the gas. Electrons can also be emitted from cathode by impact of positive ions. These electrons are called secondary electrons. Secondary electron coefficient gives electron yield per incident ion. Secondary emission is essential for self-sustaining discharges. If a steady state is assumed, then the number of ions arriving at the cathode is

$$n_t - (n_c + n_s) \tag{2.3}$$

where n_t is total number of electrons per second arriving at the anode, n_c and n_s are number of electrons per second leaving cathode due to external radiation and due to secondary emission respectively. Ionization and secondary yield coefficients [9] give

$$n_t = (n_c + n_s)e^{\alpha d}, \tag{2.4}$$

$$\gamma\big(n_t - (n_c + n_s)\big). \tag{2.5}$$

Here γ is the secondary electron yield for per incident ion. Combining these (Eq. (2.4) and Eq. (2.5)) by eliminating n_s, current in discharge gap can be written as

$$i = \frac{i_0 e^{\alpha d}}{1 - \gamma(e^{\alpha d} - 1)} \tag{2.6}$$

In Eq. (2.6), current is increased by the second term at the denominator with effect of secondary emission. Current becomes infinite when denominator equals zero. This constitutes breakdown condition as

$$\gamma(e^{\alpha d} - 1) = 1, \tag{2.7}$$

and if $\gamma \ll 1$, Townsend criterion for breakdown becomes

$$\gamma e^{\alpha d} = 1. \tag{2.8}$$

Ionization coefficient as found from experiment is in the form

$$\alpha = Ap\exp\left(-\frac{Bp}{E}\right), \tag{2.9}$$

where A and B are constants that depend on gas type, p is pressure and E is electric field. This value can be written considering number of ionization collisions in distance dx as

$$\alpha dx = \frac{dx}{\lambda} exp\left(-\frac{\varepsilon_i}{qE\lambda}\right), \tag{2.10}$$

where ε_i is ionization threshold energy of gas atoms and λ is the mean free path of electrons. Mean free path is inversely related to pressure. dx/λ refers to number of collisions in distance dx and exponential term is ionization probability. Using breakdown criterion (Eq. (2.7)) and E for parallel electrodes gives

$$\alpha d = ln\ (1 + \frac{1}{\gamma}), \tag{2.11}$$

$$Apdexp\left(-\frac{Bpd}{V_B}\right) = ln\ (1 + \frac{1}{\gamma}). \tag{2.12}$$

DC breakdown voltage becomes

$$V_B = \frac{Bpd}{\ln\ (Cpd)}, \tag{2.13}$$

where C is taken as another constant as

$$\frac{A}{\ln\ (1 + \frac{1}{\gamma})}. \tag{2.14}$$

Value of V_B depends on product of gas pressure and distance between the electrodes. This relation holds for limited range of field and pressure values. For range of values of pd, V_B is minimum for certain gas type. For very low values of product pd as breakdown voltage goes infinity, no breakdown is possible for the gas when

$$pd < \tfrac{1}{A}\ln\ (1 + \tfrac{1}{\gamma}). \tag{2.15}$$

V_B versus pd curve known as Paschen's curve shows these characteristics.

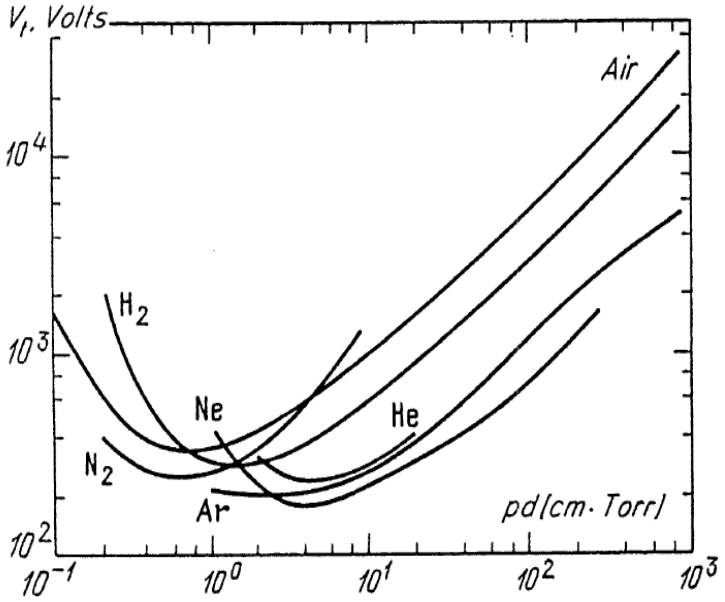

Figure 2.1. Paschen curves for different gasses [10].

For lower values of pressure, there are not enough collisions and higher voltage is needed for breakdown. For higher values of pressure, smaller mean free path makes collisions frequent but energy gain of electrons is not enough. Thus, higher values of breakdown voltage are observed. This explains the minimum point in the Paschen curve.

2.2. Glow Discharge

After breakdown voltage is reached, steady state of Townsend regime is disturbed. Transition to glow region occurs where current or discharge becomes self-sustaining. Glow discharge can be seen as starting point where many plasma properties are observed, such as potential drop at the walls, quasi-neutrality of the bulk and the nature of collisions.

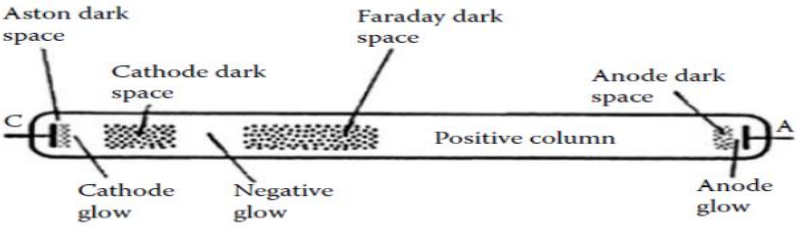

Figure 2.2. Glow discharge layers [11].

Self-sustaining behavior of glow discharge regime depends on how particle lost to the walls is compensated by collisional processes. Secondary electrons produced by ion impact at the cathode and ionization collisions between electron and neutrals are determining factors for the glow regime. Characteristic dark and luminous layers are formed depending on gas type. Positive space charge forms in cathode region and electrons are accelerated by resulting electric field. Cathode glow is mostly due to recombination of positive ions with electrons. After cathode glow, the cathode dark space forms where electrons continue to gain energy and cause ionizing collisions. In this region very low excitation cross-sections results in dark region. Negative glow is resulted from excitation reactions caused by energetic electrons. This region along with the cathode dark space form main ionization source of the discharge. After negative glow, as a result of decreasing field strength, energy gain of electrons reduces and energy losses in negative glow results in Faraday dark space. Decrease in the density of electrons results in positive column where net charge density becomes close to zero. Positive column is where the quasi-neutrality is mainly observed. When the electrode distance is made smaller, positive column gets smaller and eventually removed along with the Faraday dark space. Discharge can maintain only with the cathode region containing negative glow. Closer to anode increasing electric field accelerating electrons results in anode glow. Further increase of the current result in transitions to abnormal glow and later arc discharge regimes. Ohm's law for the discharge circuit [10] is given by

$$\varepsilon = V + i\Omega, \tag{2.16}$$

where ε is the supplied voltage.i,Ω are the discharge current and resistance of the system respectively and V is the voltage between the electrodes. Intersection of straight line arising from this equation with voltage-current graph gives the value of current and voltage of the discharge. This line is known as load line. Steepness of the line is determined by resistance for a fixed electromotive force supplied from a power source.

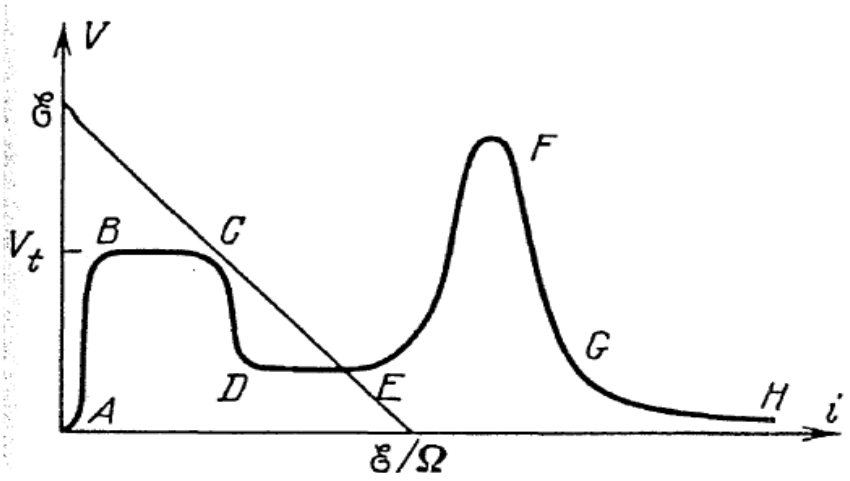

Figure 2.3. Voltage-current characteristics of discharge. A: Non-self-sustaining discharge. BC: Townsend discharge. CD: Subnormal glow. DE: Normal glow. EF: Abnormal glow. FG: Transition to arc. GH: Arc discharge [10].

Very high resistance and low current corresponds to dark discharge and Townsend regime. After further decreasing resistance, transition to normal glow discharge from low current region called subnormal glow occurs. In normal glow region, there is constant current density while the current increases. After whole surface of cathode is covered by discharge, abnormal glow region begins where current density and current increase with voltage. Further increase of current after abnormal glow results in transition to arc regime where heating of the cathode becomes important. In the arc regime, discharge reaches higher pressure values and higher current density is obtained with relatively low voltage. Main source of electrons in the arc regime is the thermionic emission and potential drop at the cathode is reduced compared to glow regime.

2.3. Debye Shielding

Collective behavior of charged particles is one of the distinct properties of the plasmas and characteristic length scale over which this is observed is known as Debye length. This can be explained by potential or electric field around a single charge in plasma. When same equilibrium density is assumed for both ions and electrons, where electrons follow Boltzmann distribution, one dimensional Poisson's equation becomes

$$\frac{\mathrm{d}^2V}{\mathrm{dx}^2} = \frac{en_0}{\varepsilon_0}\left(exp\left(-\frac{eV}{kT_e}\right) - 1\right). \tag{2.17}$$

Expanding exponential where $eV \ll kT_e$ and omitting higher order terms, Eq. (2.17) can be written as

$$\frac{\mathrm{d}^2V}{\mathrm{dx}^2} = \frac{n_0e^2}{\varepsilon_0 kT_e}V, \tag{2.18}$$

which has the solution

$$V = V_0 exp\left(\frac{-|x|}{\lambda_D}\right), \tag{2.19}$$

where

$$\lambda_D = \sqrt{\frac{\varepsilon_0 kT_e}{n_0e^2}}. \tag{2.20}$$

Here $\lambda_D$is the Debye length. It characterizes the screening distance of potential where it goes off exponentially. Depending on the Debye length, two fundamental conditions for plasma state can be given. For collective behavior to be observed, there should be enough number of particles in Debye sphere. This also gives condition for plasma state as

$$n\frac{4}{3}\pi\lambda_D^3 \gg 1, \tag{2.21}$$

where n is the density. Moreover; length scale in which plasma is observed to be quasi-neutral should be much greater than the Debye length as

$$\lambda_D \ll L. \tag{2.22}$$

2.4. Sheath Formation

When a neutral substrate inserted in plasma or near the insulating walls, a sheath region with a negative potential to the bulk develops. At first, electron flux to the wall is much greater than ion flux because of the temperature and mass difference. This results in negative charge which attracts ions and repels electrons. Thus, a positive space charge is formed around wall. Later, ion and electron currents to the wall are balanced and value of potential that this is observed is called as floating potential. Potential at the bulk is known as space potential. Electrons are accelerated to the bulk and ions to the wall by the potential difference. Potential of the sheath region can be given by balancing the fluxes to the wall as

$$n_0 v_e exp\left(\frac{e\phi_w}{kT_e}\right) = n_0 v_i exp\left(\frac{-e\phi_w}{kT_i}\right). \tag{2.23}$$

Here, same equilibrium density is taken for electrons and ions for the bulk. Both electrons and ions follow Boltzmann distribution. $v_{e,i}$ are thermal velocities. ϕ_w is the wall potential. If electron and ion temperature are assumed to be equal, Eq. (2.23) becomes

$$\left(\frac{m_i}{m_e}\right)^{1/2} = exp\left(\frac{-2e\phi_w}{kT_e}\right) \tag{2.24}$$

taking logarithm of both sides gives

$$\phi_w = -\frac{kT_e}{4e} ln\left(\frac{m_i}{m_e}\right). \tag{2.25}$$

Wall potential is negative, depends on electron temperature and ratio of the masses. Using continuity equation in one dimension where there is no time dependence, density conservation for ions coming to sheath region becomes

$$n_i(x)u_x = n_0u_0, \tag{2.26}$$

where n_0 and u_0 are bulk density and flow velocity of ions coming to the sheath respectively. Here, n_i and u_x are density and flow velocity in the sheath region. Energy conservation gives

$$\frac{1}{2}m_iu_0^2 = \frac{1}{2}m_iu_x^2 + e\phi(x), \tag{2.27}$$

where e is the elementary charge. Then, ion velocity in sheath region becomes

$$u_x = \left(u_0^2 - \frac{2e\phi(x)}{m_i}\right)^{1/2}. \tag{2.28}$$

Thus, ion density in sheath is

$$n_i(x) = \frac{n_0}{\left(1 - \frac{2e\phi(x)}{m_iu_0^2}\right)^{1/2}} \tag{2.29}$$

Electrons facing potential barrier in the sheath is taken to follow Boltzmann distribution as

$$n_e(x) = n_0exp\left(\frac{e\phi(x)}{T_e}\right). \tag{2.30}$$

Poisson's equation becomes

$$\frac{d^2\phi}{dx^2} = \frac{en_0}{\varepsilon_0}\left[exp\left(\frac{e\phi(x)}{T_e}\right) - \left(1 - \frac{2e\phi(x)}{m_iu_0^2}\right)^{-1/2}\right] \tag{2.31}$$

This gives a non-linear system. By taking $e\phi \ll T_e$ and $e\phi \ll m_iu_0^2$, terms on the right can be expanded as

$$\exp\left(\frac{e\phi}{T_e}\right) \cong 1 + \frac{e\phi}{T_e} + 0[\left(\frac{e\phi}{T_e}\right)^2] \tag{2.32}$$

$$\left(1-\frac{2e\phi}{m_i u_0^2}\right)^{-1/2} \cong 1+\frac{e\phi}{m_i u_0^2}+\ O[\left(\frac{e\phi}{T_e}\right)^2]. \tag{2.33}$$

Putting these (Eq. (2.32) and Eq. (2.33)) in Poisson's equation and omitting higher order terms [12], Eq. (2.31) becomes

$$\frac{d^2\phi}{dx^2}=\frac{\phi}{\lambda_D^2}\left(1-\frac{v_s^2}{u_0^2}\right), \tag{2.34}$$

where λ_D,v_s are Debye length and ion sound speed given as $(T_e\ /\ m_i)^{1/2}$ respectively. Using the definition of Mach number giving ratio of speed to sound speed ($M=(\frac{u_0}{v_s})$), Eq. (2.34) can be written as

$$\frac{d^2\phi}{dx^2}=\frac{\phi}{\lambda_D^2}\left(1-\frac{1}{M^2}\right). \tag{2.35}$$

Eq. (2.35) gives non-oscillatory solutions for $M^2>1$, which also gives the condition known as Bohm sheath criterion that ions come into sheath with a greater speed than ion sound speed that is also called here as Bohm velocity. Poisson's equation can be written again to calculate current that can be drawn if wall potential is made arbitrarily large, in the form

$$\frac{d^2\chi}{dx^2}=\frac{1}{\lambda_D^2}\left[exp(\chi)-\left(1-\frac{2\chi}{M^2}\right)^{-1/2}\right], \tag{2.36}$$

where $\chi=e\phi_w\ /\ T_e$. Neglecting electron density near the wall and taking $e|\phi_w|\ /\ T_e \gg 1$, Eq. (2.36) [12] becomes

$$\frac{d^2\chi}{dx^2}=\frac{-M}{\lambda_D^2}\frac{1}{(-2\chi)^{1/2}}, \tag{2.37}$$

Integrating after multiplying both sides with $d\chi\ /\ dx$ gives

$$\lambda_D\frac{d\chi}{dx}=M^{1/2}2^{3/4}\chi^{1/4}. \tag{2.38}$$

Integrating once more to an arbitrary position d Eq. (2.38) becomes

$$\int_0^d dx = \int_{\chi_w}^{\chi} \frac{\lambda_D d\chi}{M^{1/2} 2^{3/4} \chi^{1/4}}. \tag{2.39}$$

Neglecting the upper limit on right-hand side and taking the square of both sides, solution can be written as

$$Md^2 = \frac{\lambda_D^2}{2^{3/2}} \frac{16}{9} \chi_w^{3/2}. \tag{2.40}$$

After putting Mach number $M = u_0 \,/\, v_s$ and $\chi_w = e\phi_w \,/\, T_e$ in Eq. (2.40), ion current density ($J = n_i e u_0$) to the wall becomes

$$J = \frac{4}{9}\left(\frac{2e}{m_i}\right)^{1/2} \frac{\varepsilon_0 \phi_w^{3/2}}{d^2}. \tag{2.41}$$

This relation (Eq. (2.41)) is known as Child-Langmuir law gives the ion current density in space charge limit.

2.5. Plasma Probes

Probes are used for plasma diagnostics using voltage-current characteristics. Measurements give information about temperature and density. By inserting the probe, a bias voltage is introduced. Reference could be one of the electrodes or another probe. Bias voltage [13] is given by

$$V = V_p + V_s, \tag{2.42}$$

where V_p and V_s are probe and plasma potential respectively. Different probe voltages determine the amount of current drawn. There are ion and electron saturations and a region in between. For $V \ll V_s$, probe potential can produce negative space charge limit and ion saturation current is reached. Point where probe potential is zero corresponds to floating potential resulting from zero net current to probe. For $V > V_s$, there is electron saturation. For the region between floating and plasma potential, electrons are repelled by the potential. Electrons having enough energy,

$v > \left(2e|V_p|/m\right)^{1/2}$, can reach the probe. Considering drift velocity in one dimension, electron current to the probe [14] is calculated by

$$I_e = en_eA \int_{-\infty}^{\infty} dv_x \int_{-\infty}^{\infty} dv_y \int_{\left(\frac{2e|V_p|}{m}\right)^{1/2}}^{\infty} f\left(v_x, v_y, v_z\right) v_z dv_z \tag{2.43}$$

Here A is the effective area of the probe. $f\left(v_x, v_y, v_z\right)$ is the Maxwellian velocity distribution given by

$$\left(\frac{m}{2\pi kT_e}\right)^{3/2} exp\left(-\frac{m(v_x^2 + v_y^2 + v_z^2)}{2kT_e}\right). \tag{2.44}$$

Then, electron current becomes

$$I_e = \frac{en_e < v_e >}{4} Aexp\left(\frac{eV_p}{kT_e}\right), \tag{2.45}$$

where average velocity $< v_e >$ is given as

$$v_e = \left(\frac{8kT_e}{\pi m}\right)^{1/2}. \tag{2.46}$$

After taking logarithm Eq. (2.46) becomes

$$lnI_e = \frac{eV_p}{kT_e} + constant. \tag{2.47}$$

Electron temperature T_e can be determined from slope of the Eq. (2.47). Using electron temperature other properties such as plasma density, density of electrons and ions and current density of ions can be found. Electron saturation current is calculated by taking the lower limit in the third integral in Eq. (2.43) as zero, which is given by

$$I_e = \frac{en_e < v_e >}{4} A. \tag{2.48}$$

Using Bohm velocity u_B given by $(kT_e/m_i)^{1/2}$, ion saturation current density can be written as

$$J_i = en_i u_B \tag{2.49}$$

Multiplying Eq. (2.49) with effective probe area gives ion saturation current. Potential at the sheath edge making ions reach Bohm speed is given by

$$\phi_s \approx -\frac{1}{2}\frac{kT_e}{e}. \tag{2.50}$$

Using ϕ_s and assuming Boltzmann distribution for electrons, density at the sheath edge can be written as

$$n_s = n_0 \exp\left(e\phi_s/kT_e\right). \tag{2.51}$$

Eq. (2.50) and Eq. (2.51) give

$$n_s \approx 0.5 n_0, \tag{2.52}$$

where n_0 is the plasma density. In pre-sheath region density of electrons and ions can be taken as approximately equal. Then, ion saturation current can be given as

$$I_B = \frac{1}{2} n_0 eA \left(\frac{kT_e}{m_i}\right)^{1/2}. \tag{2.53}$$

When electron temperature is known, plasma density is calculated by I_B that is also called as Bohm current [12].

2.6. Diffusion

Collisional diffusion is considered as random walk process where mean free path of the molecules is the step size. Diffusion coefficient relates mean square distance with average time between collisions. If a net flux around a point in one dimension is considered as

$$\Gamma = \Gamma_+ - \Gamma_-, \tag{2.54}$$

where Γ_+, Γ_- are fluxes to right and left respectively. In the time interval Δt, where half of the particles travels to each direction, flux to right is

$$\frac{1}{2}\int_{x_0-\Delta x}^{x_0}\frac{n(x)}{\Delta t}dx, \tag{2.55}$$

where *n*, x_0 are the density and reference point respectively. Expanding density *n(x)* in Taylor series, Eq. (2.55) becomes

$$\frac{1}{2}\int_{x_0-\Delta x}^{x_0}\frac{dx}{\Delta t}\left[n(x_0)+(x-x_0)\frac{dn}{dx}\right], \tag{2.56}$$

where higher order terms are omitted. Thus, particle flux to right is given by

$$\Gamma_+ = \frac{1}{2\Delta t}\left[n(x_0)\Delta x-\frac{\Delta x^2}{2}\frac{dn}{dx}\right]. \tag{2.57}$$

Similarly, flux to left is found as

$$\Gamma_- = \frac{1}{2}\int_{x_0}^{x_0+\Delta x}\frac{n(x)}{\Delta t}dx = \frac{1}{2\Delta t}\left[n(x_0)\Delta x+\frac{\Delta x^2}{2}\frac{dn}{dx}\right]. \tag{2.58}$$

Therefore, net flux is

$$\Gamma = \frac{-(\Delta x)^2}{2\Delta t}\frac{dn}{dx} = -D\nabla n. \tag{2.59}$$

This is the Fick's diffusion law giving net flux dependent on density gradient, taking diffusion coefficient D as $\Delta x^2/2\Delta t$. In a weakly ionized plasma where there is no magnetic field, flux of species can be determined by momentum balance equation given by

$$mn\frac{d\mathrm{v}}{dt} = qnE-\nabla p-mn\nu\mathrm{v}. \tag{2.60}$$

Considering a steady state where $d\mathrm{v}/dt$ vanishes and isothermal system where collisions are dominant as collision frequency is much greater than the time scale that density changes and where $\nabla p = kT\nabla n$ [12], Eq. (2.60) gives flow velocity as

$$\mathrm{v} = \frac{q}{mv}E - \frac{kT}{mv}\frac{\nabla n}{n}, \tag{2.61}$$

Thus, particle flux becomes

$$\Gamma = n\mu E - D\nabla n, \tag{2.62}$$

where μ, D are mobility (q/mv) and diffusion coefficient (kT/mv) respectively. In plasmas, diffusion and mobilities of electrons and ions are different because of mass difference. Electrons being more mobile diffuse faster and leaves a positive space charge. This results in an electric field known as ambipolar that confines electrons and accelerates ions oppositely. Condition of equal fluxes ($\Gamma_e = \Gamma_i$) required by quasi-neutrality is

$$-n\mu_e E - D_e\nabla n = n\mu_i E - D_i\nabla n. \tag{2.63}$$

This gives ambipolar electric field as

$$E = \frac{D_i - D_e}{\mu_i + \mu_e}\frac{\nabla n}{n}. \tag{2.64}$$

Using this field in flux for either ions and electrons gives ambipolar flux as

$$\Gamma_a = -\frac{\mu_i D_e + \mu_e D_i}{\mu_i + \mu_e}\nabla n, \tag{2.65}$$

where ambipolar diffusion coefficient is

$$D_a = \frac{\mu_i D_e + \mu_e D_i}{\mu_i + \mu_e}. \tag{2.66}$$

Taking mobility of ions much smaller than electron mobility and assuming equal temperatures, ambipolar diffusion coefficient can be approximated as

$$D_a \approx 2D_i . \tag{2.67}$$

Therefore, diffusion of ions is multiplied by ambipolar electric field and value of D_a is governed by diffusion of ions [12].

2.7. Electron Plasma Oscillations

As stated by quasi-neutrality, any changes of equilibrium values of field and potential are opposed by motion of charged particles in plasma with the effect of long-range Coulomb forces. As being more mobile, electrons response much more effectively than ions to small changes. Considering only first order perturbations around equilibrium density and after omitting higher order terms, continuity equation in one dimension is written as

$$\frac{\partial n}{\partial t} + n_0 \frac{\partial v}{\partial x}, \tag{2.68}$$

where n_0, n are equilibrium density and first order perturbation respectively and where v is perturbed flow velocity. Momentum equation with same approximations becomes

$$m_e n_0 \frac{\partial v}{\partial t} = n_0 e \frac{\partial V}{\partial x} - \gamma T_e \frac{\partial n}{\partial x}, \tag{2.69}$$

where γ is the specific heat ratio (C_p / C_v) depending on degrees of freedom and equals three for one dimension and V is the perturbed potential given by Poisson's equation as

$$\frac{d^2 V}{dx^2} = \frac{e}{\varepsilon_0} n. \tag{2.70}$$

Here equilibrium densities of electrons and ions are taken as equal. If equilibrium thermal motion is ignored, combining these equations by taking time derivative of

continuity equation and putting value of $\partial v / \partial t$ from Eq. (2.69), equation for perturbed density can be written as

$$\frac{\partial^2 n}{\partial t^2} + \left(\frac{n_e e^2}{m_e \varepsilon_0}\right) n = 0, \tag{2.71}$$

where electron plasma frequency is given by

$$w_{pe} = \left(\frac{n_e e^2}{m_e \varepsilon_0}\right)^{1/2}. \tag{2.72}$$

An electron with thermal velocity goes approximately distance of Debye length in one plasma period as

$$\lambda_{\mathrm{D}} = \frac{v_T}{w_{pe}}. \tag{2.73}$$

If electron temperature is not neglected, independent density fluctuations of electrons couple with the thermal motion. This gives the dispersion relation relating wave vector to frequency of oscillations. To do this, fluid equations are used with Maxwell's equations. Considering only electric field, continuity and momentum equations for the electrons become

$$\frac{\partial n_e}{\partial t} + \nabla \cdot n_e v_e = 0, \tag{2.74}$$

$$m_e n_e \left(\frac{\partial v_e}{\partial t} + v_e \cdot \nabla v_e\right) = -e n_e E - \gamma T_e \nabla n_e. \tag{2.75}$$

Gauss's Law is

$$\nabla \cdot E = \frac{\rho_p + \rho_f}{\varepsilon_0}, \tag{2.76}$$

where ρ_p, ρ_f are polarization charge density due to density perturbation and free charge density respectively. Assuming wave-like solutions [12] as

$n_e = \bar{n}\exp(ik \cdot r - iwt)$ where k is wave vector and using only first order perturbations as before continuity equation gives

$$-iw\tilde{n}_e + in_0 k \cdot \tilde{v}_e = 0, \tag{2.77}$$

where n_0, $\tilde{n}_e$, $\tilde{v}_e$ are equilibrium density, first order perturbations of density and velocity for electrons respectively. Eq. (2.75) gives velocity as

$$\tilde{v}_e = \frac{e\tilde{E}}{iwm_e} + \frac{\gamma T_e}{wm_e} k \frac{\tilde{n}_e}{n_0}, \tag{2.78}$$

where $\tilde{E}$ is first order perturbation of electric field. Using this value in Eq. (2.77), electron polarization density takes the form

$$\tilde{n}_e = \frac{-ik \cdot \tilde{E}}{1 - 3k^2 \mathrm{v}_T / 2w^2} \frac{n_0 e}{m_e w^2}, \tag{2.79}$$

where thermal velocity of electron is taken as $(2T_e/m_e)^{1/2}$. Eq. (2.79) gives the density perturbation along electric field. Using this value, Gauss's law (Eq. (2.76)) becomes

$$\nabla \cdot \varepsilon_0 \tilde{E} \left(1 - \frac{w_{pe}^2}{w - (3/2)k\mathrm{v}_T^2}\right) = \tilde{\rho}_f, \tag{2.80}$$

where $\tilde{\rho}_f$ is perturbed free charge density. Thus, electrostatic dielectric constant of plasma can be written as

$$\varepsilon(k, w) = \varepsilon_0 \left(1 - \frac{w_{pe}^2}{w - (3/2)k\mathrm{v}_T^2}\right) \tag{2.81}$$

Dispersion relation giving frequency for the normal mode oscillations is the condition of $\varepsilon(k, w) = 0$. This gives

$$w^2 = w_{pe}^2 + 3k^2 \mathrm{v}_T^2. \tag{2.82}$$

Eq. (2.82) is known as Bohm-Gross dispersion relation. Here ions are considered as fixed uniform background and only electron oscillations along electric field (longitudinal) is considered.

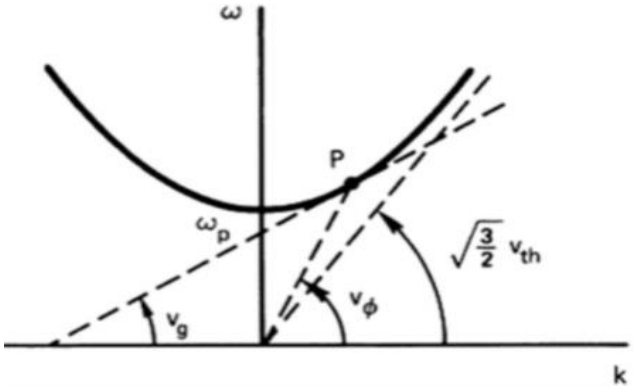

Figure 2.4. Dispersion curve [12].

Slope of any line from origin to any point on the dispersion curve gives phase velocity (v_ϕ). Group velocity is given by the slope of the tangent to any point on the curve as

$$v_g = \frac{dw}{dk} = \frac{3}{2}\frac{v_T^2}{v_\phi} \ . \tag{2.83}$$

Information is carried at the order of thermal velocity. For higher electron temperatures this is closer to thermal velocity. If thermal motion is ignored, information is not carried at all as group velocity, $v_g = 0$ [12, 15].

CHAPTER 3

NUMERICAL METHOD

3.1. Particle in Cell Method

Numerical methods used in plasma simulations have different approaches to solve linear Boltzmann equation for particle distribution functions in six-dimensional position and velocity phase space given as

$$\frac{\partial f(\vec{r},\vec{\mathrm{v}},t)}{\partial t}+\vec{\mathrm{v}}\cdot\nabla_r f(\vec{r},\vec{\mathrm{v}},t)+\vec{a}\cdot\nabla_{\mathrm{v}} f(\vec{r},\vec{\mathrm{v}},t)=\left(\frac{\partial f}{\partial t}\right)_{coll} \tag{3.1}$$

Here distribution function f can be defined as probability of finding particles in unit volume where number of particles in the infinitesimal volume element $d^3r d^3\mathrm{v}$ can be written as

$$f(r,\mathrm{v})d^3r d^3\mathrm{v}. \tag{3.2}$$

Macroscopic quantities such as particle density, drift velocity and mean energy are calculated from velocity moments of distribution function [16] as

$$n(r)=\int d^3\mathrm{v}\, f(r,\mathrm{v}) \tag{3.3}$$

$$v(r)=\frac{1}{n(r)}\int d^3\mathrm{v}\, f(r,\mathrm{v})\,\mathrm{v} \tag{3.4}$$

$$\varepsilon(r)=\frac{1}{n(r)}\int d^3\mathrm{v}\, f(r,\mathrm{v})\frac{1}{2}m\mathrm{v}^2 \tag{3.5}$$

By excluding collisional term on the right-hand side of Eq. (3.1), PIC method is shown to be equivalent to solving Vlasov equation which considering only one dimension and electric field is written as

$$\frac{\partial f_s}{\partial t} + \mathrm{v}\frac{\partial f_s}{\partial x} + \frac{q_s E}{m_s}\frac{\partial f_s}{\partial \mathrm{v}}, \tag{3.6}$$

where m_s and q_s are mass and charge of the given particle species. Eq. (3.6) describes the evolution of particle trajectories by external forces. In particle in cell method, finite sized computational particles are used and their trajectories are followed to sample the phase space distribution.

3.1.1. Particle Weighting

Super particles used in the simulation represent number of real particles that is called as particle or specific weight. They can be seen as finite elements in phase space that distribution function of charged species [17] is given by superposition of these elements. Order of the weighting method determines the accuracy of the forces on particles and of the densities and fields on grid points.

Distribution function of the computational or super particles in one dimension [17] is written as

$$f_p(x,\mathrm{v},t) = N_p S_x\left(x - x_p(t)\right) S_{\mathrm{v}}\left((\mathrm{v} - \mathrm{v}_p(t)\right) \tag{3.7}$$

where S_x and S_{v} are shape functions in spatial and velocity space respectively. Here N_p is the specific weight. Velocity space shape function is Dirac delta function as particles represented by one super particle are considered to have same speed. Spatial shape functions are determined from different orders of basic splines as

$$S_x(x - x_p) = \frac{1}{\Delta_p} b_l\left(\frac{x - x_p}{\Delta_p}\right). \tag{3.8}$$

Here Δ_p is the length scale of the super particle. Most commonly used weighting methods are zero and first order weightings that are known as nearest-grid-point (NGP) and cloud in cell (CIC) respectively. Zeroth order weighting gives nearest grid point (NGP) scheme where particle densities are weighted to one nearest grid point and same grid contributes to fields at particle positions. First order weighting gives

CIC method which is also used in this study and usually preferred because of reduced noise compared to NGP scheme.

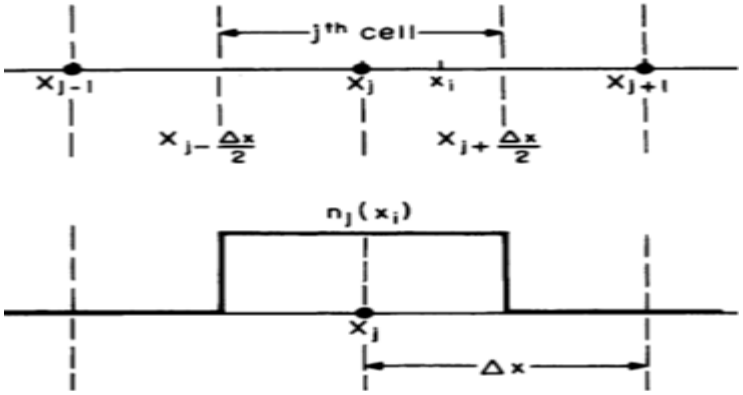

Figure 3.1. NGP scheme [18].

As mentioned before, first order weighting is resulted from using higher order interpolation method and it is used to reduce density and field fluctuations in the NGP scheme. Charge densities are accumulated at two grid points rather than one as

$$q_j = q_i \left(\frac{X_{j+1} - x_i}{\Delta x} \right), \tag{3.9}$$

$$q_{j+1} = q_i \left(\frac{x_i - X_j}{\Delta x} \right). \tag{3.10}$$

Here q_j and q_{j+1} are charges on respective grid points, x_i and $X_{j,j+1}$ are the particle and grid point positions respectively.

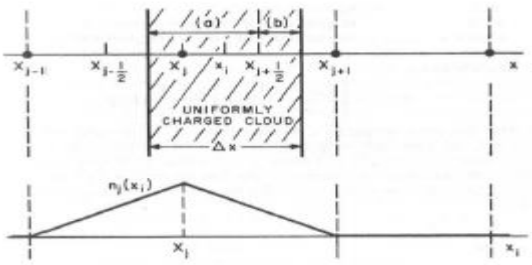

Figure 3.2. CIC scheme [18].

Higher order interpolations give more accurate results with fewer particles, but they are computationally more involved.

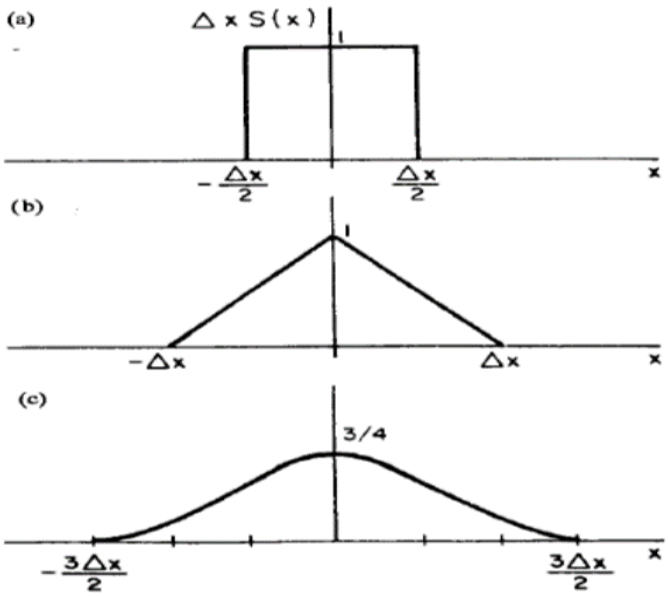

Figure 3.3. Various weighting functions a) Zero-order (NGP), b) First-order (CIC), c) Second-order (parabolic) [19].

3.1.2. Equation of Motion

Above chosen form of distribution function for the computational particles satisfies the moments of one-dimensional Vlasov equation. First order spatial and velocity moments result in Newton's equations of motion.

$$\frac{dv}{dt} = \frac{F}{m}, \tag{3.11}$$

$$\frac{dx}{dt} = v. \tag{3.12}$$

F is the force on particles, m is the mass, x and v are position and velocity respectively. There are several time integration methods. Commonly preferred method in PIC simulations is the leapfrog integration. It is an explicit method where velocities are updated using forces at the older time steps and it is second order accurate where velocities are calculated half time steps whereas positions and fields are calculated in

integer time steps. It can be seen as velocities and positions following each other and jumping over at half time steps as name suggests as leapfrog. It is derived from Taylor series as

$$x(t_n + \Delta t) = x(t_n) + v(t_n)\Delta t + \frac{1}{2}a(x_n, t_n)\Delta t^2 + O(\Delta t^3) \tag{3.13}$$

where a is acceleration. Velocity at half time step is used at Eq. (3.16) as

$$v(t_{n+1/2}) = v(t_n) + \frac{1}{2}a(x_n, t_n)\Delta t\,, \tag{3.14}$$

that gives

$$x(t_n + \Delta t) = x(t_n) + v(t_n + \Delta t/2)\Delta t + O(\Delta t^3)\,. \tag{3.15}$$

In implementation, first step is finding velocity at half time step back using initial force value. After this, algorithm becomes

$$v_{n+1/2} = v_{n-1/2} + a_n\Delta t\,, \tag{3.16}$$

$$x_{n+1} = x_n + v_{n+1/2}\Delta t\,. \tag{3.17}$$

Leapfrog is usually chosen over higher order methods as it couples well with the field equations and gives accurate results while being relatively faster. Another common integration method is velocity Verlet which is also used in this study. Velocity Verlet is second order accurate as leapfrog and it is an implicit method where velocities and positions are calculated at same time step as

$$x_{n+1} = x_n + v_n\Delta t + \frac{1}{2}a_n\Delta t^2 \tag{3.18}$$

$$v_{n+1} = v_n + \frac{1}{2}(a_n + a_{n+1})\Delta t\,. \tag{3.19}$$

Because of being implicit, it allows higher values for time step than leapfrog but could be more involved as it requires force and position on the same time step to update velocities [20]. For stability of explicit leapfrog scheme, time step should satisfy Courant (CFL) condition known as

$$\Delta t \leq \frac{\Delta x}{\mathrm{v}_{\max}}, \tag{3.20}$$

where $\mathrm{v}_{\max}$ is the maximum speed of particles. Time step should also resolve electron plasma oscillations as $w_{pe}\Delta t \leq 2$. For more accuracy smaller limit could be used as

$$w_{pe}\Delta t \leq 0.2 \tag{3.21}$$

w_{pe} is the electron plasma frequency,

$$\mathrm{w}_{\mathrm{pe}} = \left(\frac{e^2 n_e}{\varepsilon_0 m_e} \right)^{1/2} \tag{3.22}$$

For collisions, modification of classical leap-frog integration [21] is possible to get position and velocity vectors at same time steps giving accurate results with Monte Carlo collisions.

3.1.3. Field Equations

After finding densities on grid points, potential and related fields are calculated using Maxwell's equations and chosen discretization method in space. In this study, only electric field is considered requiring solution of Poisson equation in one dimension as

$$\frac{\partial^2 V}{\partial x^2} = -\frac{\rho}{\varepsilon_0}, \tag{3.23}$$

where V is the potential and ρ is the total charge density. Discretization of this equation by finite difference takes the form

$$\frac{V_{i+1}-2V_i+V_{i-1}}{\Delta x^2}=-\frac{\rho_i}{\varepsilon_0}, \tag{3.24}$$

which gives system of equations

$$\begin{bmatrix} 2 & -1 & 0 & \cdots & 0 \\ -1 & 2 & -1 & \ddots & \vdots \\ 0 & \ddots & \ddots & \ddots & 0 \\ 0 & \ddots & -1 & 2 & -1 \\ 0 & \cdots & 0 & -1 & 2 \end{bmatrix} \begin{bmatrix} V_2 \\ V_3 \\ \vdots \\ V_{N-2} \\ V_{N-1} \end{bmatrix} = \begin{bmatrix} (\rho_2/\varepsilon_0)\Delta x^2+V_1 \\ (\rho_3/\varepsilon_0)\Delta x^2 \\ \vdots \\ (\rho_{N-2}/\varepsilon_0)\Delta x^2 \\ (\rho_{N-1}/\varepsilon_0)\Delta x^2+V_N \end{bmatrix} \tag{3.25}$$

There are N-2 equations for inner nodes where Dirichlet boundary conditions are applied on first and last of the inner nodes. There are various methods to solve such system of equations. This is a sparse tridiagonal system that is easily solved by Gaussian elimination where forward elimination and backward substitution are applied. After calculating potential on the grids, electric field for inner nodes is calculated by second order central difference as

$$E_i=-\frac{V_{i+1}-V_{i-1}}{2\Delta x}. \tag{3.26}$$

For field on the first and last grid point, forward difference and backward difference are used respectively. Grid fields are interpolated to particle positions by using the same interpolation function used in charge assignment that is

$$S(x_i-x_p)=\begin{cases} 1-\frac{|x_i-x_p|}{\Delta x} & |x_i-x_p|\le\Delta x \\ 0 & \text{else} \end{cases}, \tag{3.27}$$

where x_i and x_p are grid point and particle positions respectively. This gives field on particle positions as

$$E_p=\frac{x_p-x_i}{\Delta x}E_{i+1}+\frac{x_{i+1}-x_p}{\Delta x}E_i. \tag{3.28}$$

3.1.4. Particle Loading

In simulation first step is creating super particles with certain position and velocity distribution. For positions, particles can be injected from certain point or can be distributed using uniform random numbers between (0,1). Velocities can also be sampled from desired distribution or direction according to physical and geometrical considerations of the system. Common way for velocities is sampling Maxwellian distribution which is used in this study. This illustrates the elementary idea of Monte Carlo sampling where cumulative distribution function of a random variable is mapped to uniform random numbers between (0,1). Probability distribution function of a random variable can be written in any interval (*a*,*b*) and is normalized as

$$\int_a^b p(x)dx = 1\,, \tag{3.29}$$

where $p(x)dx$ gives probability of x to be between (x, x+dx). Cumulative distribution function is defined as

$$P(x) = \int_a^x p(x')dx' \tag{3.30}$$

giving probability of random variable taking a value up to x. By generating random numbers from uniform distribution between (0,1) and using invertibility of cumulative distribution function, values of random variable from desired probability density function [22] can be produced as

$$P(x) = \int_a^x p(x')dx' = R\,, \tag{3.31}$$

$$x = P^{-1}(R)\,. \tag{3.32}$$

where R is a uniform random number. Forms of probability density functions are usually known such as Maxwellian velocity distribution which can be written as

$$\frac{1}{v_t(2\pi)^{1/2}}\exp\left(-\frac{v^2}{2v_t^{\,2}}\right), \tag{3.33}$$

where v_t is the thermal velocity. To apply above basic method, P(x) should be calculated from the integral in Eq. (3.34). In this study to produce Maxwellian velocities, Box-Muller method [23] is used. General form of Gaussian distribution can be written as

$$g(t)=\frac{1}{(2\pi)^{1/2}}\exp\left(-\frac{1}{2}t^2\right). \tag{3.34}$$

Considering independent random variables in two dimensions, Eq. (3.37) takes the form

$$f(x,y)=\frac{1}{2\pi}\exp\left(-\frac{x^2+y^2}{2}\right), \tag{3.35}$$

using polar coordinates where

$$x=r\cos(\theta) \tag{3.36}$$

$$y=r\sin(\theta), \tag{3.37}$$

this becomes

$$f(r,\theta)drd\theta=\frac{1}{2\pi}\exp\left(-\frac{r^2}{2}\right)rdrd\theta. \tag{3.38}$$

There are two independent probability density functions that can be sampled with two uniform random numbers [24] as

$$\int_0^r r'\exp\left(-\frac{r'^2}{2}\right)dr'=U_1 \tag{3.39}$$

$$\int_0^{\theta} \frac{1}{2\pi} d\theta = U_2 , \tag{3.40}$$

which gives

$$r = \sqrt{-2\ln U_1} \tag{3.41}$$

$$\theta = 2\pi U_2 \tag{3.42}$$

Here U_1 and U_2 are uniform random numbers, thus velocity components become

$$x = \sqrt{-2\ln U_1}\cos(2\pi U_2) , \tag{3.43}$$

$$y = \sqrt{-2\ln U_1}\sin(2\pi U_2) \tag{3.44}$$

3.2. Collisions

In this study, collisions between charged particles and neutrals are simulated using Null collision method which is a well-known modification of direct Monte Carlo method. General idea of the direct method is determining particle free flight times based on the collision probability [25]

$$P(t) = 1 - \exp(-\nu_c t) , \tag{3.45}$$

where ν_c is the total collision frequency of particle and P(t) is probability of collision at t. Collision frequency depends on neutral density, total cross-section and energy as

$$\nu_c = n_0 \sigma_T (\mathrm{v})\mathrm{v} . \tag{3.46}$$

Here v is the magnitude of velocity. Free flight time can be determined mapping cumulative distribution function with uniform random numbers related with the probability of free flight that is the probability of not making collisions in certain time interval [26] as

$$p(t_c) = \nu_c \exp(-\nu_c t_c), \tag{3.47}$$

$$R = c(t) = \int_0^t p(t')dt' . \tag{3.48}$$

Inverting cumulative distribution function in Eq. (3.51) gives

$$t_c = -\frac{\ln R}{\nu_c}, \tag{3.49}$$

where t_c is the time between collisions and *R* is a uniform random number between (0,1). This value is determined for every particle. After free flight, type of collision is determined by checking the ratio of probability of the process to the total probability as

$$R \le \frac{1-\exp(-\nu_i t_c)}{P_t} \approx \frac{\nu_i}{\nu_c} . \tag{3.50}$$

Here ν_i is collision frequency of the process that depends on the cross-section value. If above condition is satisfied then collision of that type occurs. After that, particle is given another free flight time with another random number and tracked until next collision check and so on. Here total collision frequency of particle is taken to be constant for free flight which is not always the case due to effects of fields. This direct method could be accurate depending on the range of collision frequencies but it is not always applicable as it can be very involved as total collision frequency depends on particle energy and can be time consuming to assign a random number for probability check and free flight time to all the particles.

Addition of collisions to the system, imposes another consideration for time step as maximum collision probability for particles should be reasonably small ($\nu_c \Delta t << 1$).

3.2.1. Null Collision Method

In this method, a null process that does not have any effect on particles is introduced with a certain probability. This makes the total collision frequency independent of energy and gives maximum collision frequency [27] as

$$P_{null} = \frac{\nu_{null}}{\nu_{max}}, \tag{3.51}$$

$$\nu_{max} = \nu + \nu_{null}. \tag{3.52}$$

Maximum probability of collision is determined according to this maximum value as

$$P_{max} = 1 - \exp\left(-\nu_{max}\Delta t\right) \approx \nu_{max}\Delta t \tag{3.53}$$

In every time step (Δt), instead of checking every particle for collisions, fraction of particles for collision check is determined by

$$N_c = NP_{max}. \tag{3.54}$$

Here N and N_c are number of total and collisional particles respectively. Next step is to determine if a collisional particle makes actual collision as

$$R > \frac{1 - \exp\left(-\nu\Delta t\right)}{P_{max}} \approx \frac{\nu}{\nu_{max}}, \tag{3.55}$$

where R is a uniform random number between (0,1). If this is satisfied a null collision occurs meaning no change at all. Otherwise, particle is checked for collision type with another random number. For this, ratio of the cross-section of certain types to total cross-section is used. If number of processes excluding null is k, then selection procedure for the k-th process can be given as

$$\sum_{j=1}^{k-1}\frac{\sigma_j(\varepsilon)}{\sigma_T} < R < \sum_{j=1}^{k}\frac{\sigma_j(\varepsilon)}{\sigma_T}, \tag{3.56}$$

where σ_j is cross-section of one process depending on energy and σ_T is total cross-section. Adding a null collision process is an example of rejection method that is used

when cumulative distribution function c(x) of a random variable x is not invertible to sample probability density function in the interval (a,b). To choose a value for random variable in this interval, a uniform random number is used as

$$x = a + (b - a)R\,. \tag{3.57}$$

Then depending on the maximum value on the interval, this value is accepted only if a condition using another random number [22] is satisfied as

$$R < \frac{f(x)}{f_{\max}}\,. \tag{3.58}$$

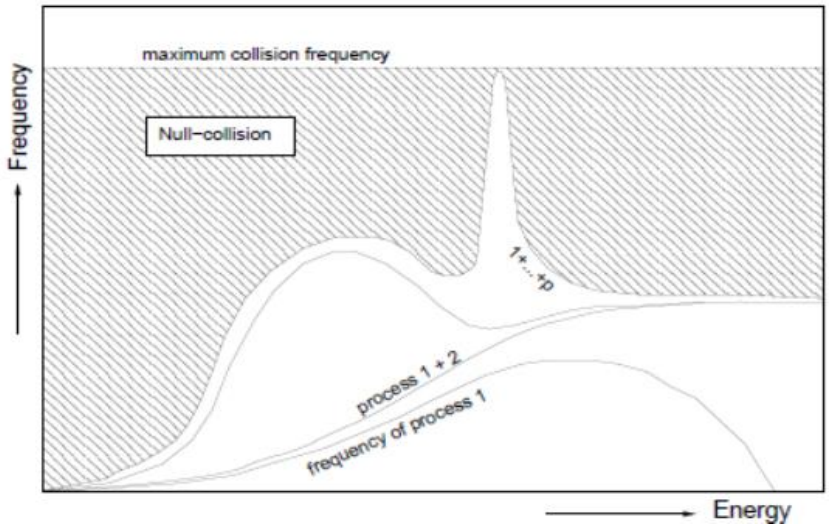

Figure 3.4. Null-collision scheme [22].

3.2.2. Calculation of Post-Collision Velocities

In electron-neutral collisions, neutrals are considered to be stationary which is a valid assumption because of mass difference. Therefore, scattering angle in the lab frame coincides with the center of mass frame. However, for ion-neutral collisions relative velocity should be used. Scattering angles for velocity transformation are calculated using differential cross-section which gives fraction of particles scattered into solid angle $d\Omega$. In general, differential cross section depends on polar and azimuthal angles

and incident particle energy. If spherical symmetry is considered, azimuthal dependence is removed. Total cross section of a process [28] becomes

$$\sigma_T(\varepsilon) = 2\pi \int_0^{\pi} \sigma(\varepsilon, \chi) \sin \chi d\chi \,, \tag{3.59}$$

where σ and χ are differential cross section and scattering angle respectively. Using differential and total cross sections, probability density function of scattering into solid angle is normalized as

$$2\pi \int_0^{\pi} \frac{\sigma(\varepsilon, \chi)}{\sigma_T(\varepsilon)} \sin \chi d\chi = 1 \,, \tag{3.60}$$

where normalized differential cross section is

$$\frac{\sigma(\varepsilon, \chi)}{\sigma_T(\varepsilon)} \,. \tag{3.61}$$

Thus, probability of scattering into solid angle is

$$\frac{\sigma(\varepsilon, \chi)}{\sigma_T(\varepsilon)} \sin \chi d\chi d\eta \,. \tag{3.62}$$

Probability density functions in both directions are sampled by uniform random numbers. For azimuthal angle

$$\int_0^{2\pi} \frac{1}{2\pi} d\eta = R \,, \tag{3.63}$$

which gives

$$\eta = 2\pi R \,. \tag{3.64}$$

For polar angle [28],

$$\frac{2\pi}{\sigma_T}\int_0^{\chi}\sigma(\varepsilon,\chi')\sin\chi' d\chi' = R\,. \tag{3.65}$$

For isotropic scattering, normalized differential cross section is taken as $1/4\pi$, then scattering angle becomes independent of energy and can be given as

$$\cos\chi = 1-2R\,. \tag{3.66}$$

For electron-neutral collisions, elastic scattering, excitation and ionization is considered. Particle energy is modified depending on the collision type. In the elastic scattering change in the electron energy is related with scattering angle [29] as

$$\Delta\varepsilon = \frac{2m}{M}(1-\cos\chi)\varepsilon_i\,, \tag{3.67}$$

where ε_i ,m and M are the energy of the incident electron, mass of the electron and the neutral respectively. Eq. (3.71) is obtained considering center of mass system coinciding with lab frame of electrons by taking neutrals at rest. Change in the kinetic energy in the center of mass frame can be written as

$$\Delta E = \frac{1}{2}\mu \mathrm{v}^2 - \frac{1}{2}\mu \mathrm{v}_r{}^2\,, \tag{3.68}$$

where μ , v, v_r are reduced mass, incident particle velocity in lab frame where target velocity is taken to be zero and relative velocity after the collision in center of mass frame respectively. Reduced mass is given by

$$\mu = \frac{mM}{m+M}\,, \tag{3.69}$$

where m , M are electron and neutral mass respectively. Taking neutrals at rest, center of mass velocity becomes

$$V_{cm} = \frac{m}{m+M}\mathrm{v}\,. \tag{3.70}$$

Then, relative velocity after collision takes the form

$$\mathrm{v}_r = \frac{m+M}{M}\mathrm{v}' - \frac{m}{M}\mathrm{v}, \tag{3.71}$$

where v' is the electron velocity after the collision in the center of mass frame. Using this in the Eq. (3.72), kinetic energy change in the center of mass frame [30] gives

$$\Delta E = (1-m/M)\varepsilon_i - (1+m/M)\varepsilon_f + 2(m/M)\sqrt{\varepsilon_i \varepsilon_f}\cos\chi \tag{3.72}$$

where ε_i, ε_f are initial and final energy of electron respectively. Taking $\Delta E = 0$ for elastic scattering with assumption of $m<<M$, formula for kinetic energy change for electrons is obtained as in Eq. (3.71).

For ionization and excitation, threshold energies are the difference. In ionization, remaining energy is equally distributed between scattered and ejected electron, and produced ion velocity is sampled using neutral temperature. Energy of ejected electron can also be determined by using experimental value and random number [31] as

$$\varepsilon_{ej} = B\tan\left[R\arctan\left(\frac{\varepsilon_{inc}-\varepsilon_{ion}}{2B}\right)\right], \tag{3.73}$$

where B is experimental parameter depending on the gas type and R is a uniform random number. ε_{inc} and ε_{ion} are incident electron and ionization energy respectively.

Pre-collision angles of the incident electron is determined as

$$\begin{bmatrix} v_x \\ v_y \\ v_z \end{bmatrix} = v\begin{bmatrix} \cos\theta \\ \sin\theta\cos\phi \\ \sin\theta\sin\phi \end{bmatrix}, \tag{3.74}$$

where v is the magnitude of the pre-collision velocity. Post collision velocity components are calculated using updated velocity magnitude and scattering angles as

$$\begin{bmatrix} v_x \\ v_y \\ v_z \end{bmatrix} = v \begin{bmatrix} \cos\chi \\ \sin\chi\cos\eta \\ \sin\chi\sin\eta \end{bmatrix}. \tag{3.75}$$

Then inverse rotations are made to transform back to lab frame. First inverse rotation is about z axes by angle θ and other is about x axes by angle ϕ [32] as

$$v_T = v \begin{bmatrix} 1 & 0 & 0 \\ 0 & \cos\phi & -\sin\phi \\ 0 & \sin\phi & \cos\phi \end{bmatrix} \begin{bmatrix} \cos\theta & -\sin\theta & 0 \\ \sin\theta & \cos\theta & 0 \\ 0 & 0 & 1 \end{bmatrix} \begin{bmatrix} \cos\chi \\ \sin\chi\cos\eta \\ \sin\chi\sin\eta \end{bmatrix}. \tag{3.76}$$

Thus, post-collision velocity components become

$$v_T = v \begin{bmatrix} \cos\theta\cos\chi - \sin\theta\sin\chi\cos\eta \\ \sin\theta\cos\phi\cos\chi + \cos\theta\cos\phi\sin\chi\cos\eta - \sin\phi\sin\chi\sin\eta \\ \sin\theta\sin\phi\cos\chi + \cos\theta\sin\phi\sin\chi\cos\eta + \cos\phi\sin\chi\sin\eta \end{bmatrix} \tag{3.77}$$

For ion-neutral collisions, magnitude of relative velocity does not change. Direction of the relative velocity is modified and post-velocity of ion is found [33] as

$$\frac{1}{2} v_r + V_{cm}, \tag{3.78}$$

where v_r is updated relative velocity. Ion and neutral mass are taken as equal and V_{cm} is center of mass velocity that is

$$V_{cm} = \frac{m_1 v_1 + m_2 v_2}{m_1 + m_2}. \tag{3.79}$$

Neutral velocity is sampled as Maxwellian for certain temperature.

3.3. Parallel Algorithm and Speed Up

Parallelization is done by using MPI in present work. There are mainly two methods namely Lagrangian and Eulerian decompositions [34]. In Lagrangian decomposition, same grid is copied for all the processors which is used in present work. MPI_Reduce function is used to accumulate charge densities in master worker which is responsible for solving for electric field. MPI_Bcast function is used to distribute field to all the processors that are responsible for their own particles. In Eulerian decomposition, processors are responsible for certain locations on the grid; therefore, grid is distributed among workers instead of particles. Increasing number of processors and speed up are not proportional. There is a limit related to part of the program that can not be parallelized known as Amdahl's law [35] that states when all the other effects such as communication time are neglected, speed up factor depending on number of processors N and non-parallelizable ratio p is given by

$$s_N = \frac{1}{p + \frac{1-p}{N}}. \tag{3.80}$$

For ideal case of infinite processors, speed up factor s_N is $1/p$.

Speed up for 4 vs. 20 cores is calculated to be about 3.12. Speed up for 4 vs. 40 cores is calculated to be about 3.84. Reduce in efficiency with increasing number of cores is obvious.

Speed up for single processor can be achieved by sub-cycling; which is used in present study for positive ions, where time-step size of slower species is certain integer multiple of faster species as ($\Delta t_{ion} = k\Delta t_{electron}$). After this, maximum collision probability of slower species is modified by same factor as ($P_{max}\Delta t_{ion}$) and also collisions for them is checked for every k time step. Another way is using different weight values [36] as higher for slower species allowing smaller number of macro particles. Fig. 3.5 shows a summary of PIC/MCC cycle for single processor.

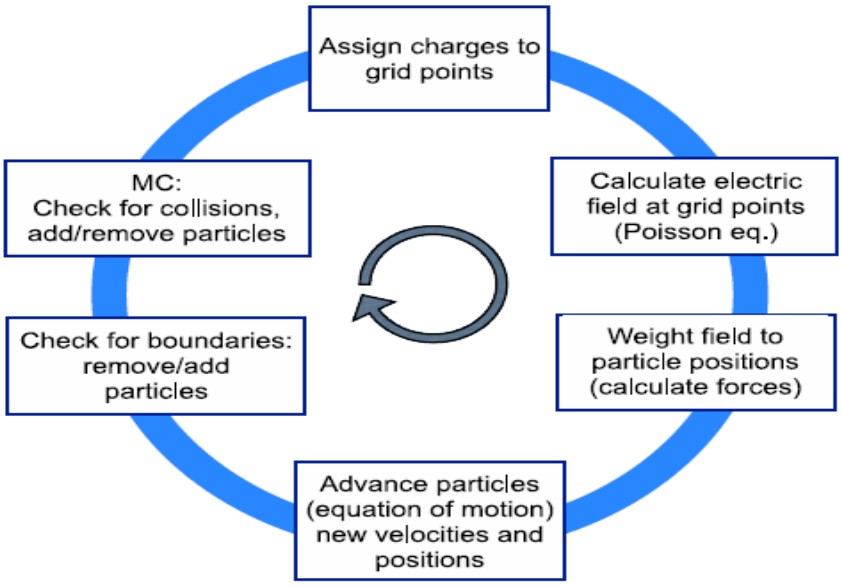

Figure 3.5. PIC-MCC cycle [37].

CHAPTER 4

VALIDATION AND RESULTS

4.1. RF Helium Discharge

Comparison is made with the parameters taken from [38]. Secondary emission, and reflection at the boundaries are ignored in these cases. Only collisions with the neutral atoms is considered. Electron-neutral collisions are elastic, single excitation, triple excitation and ionization. For ions, isotropic and backward scattering are considered.

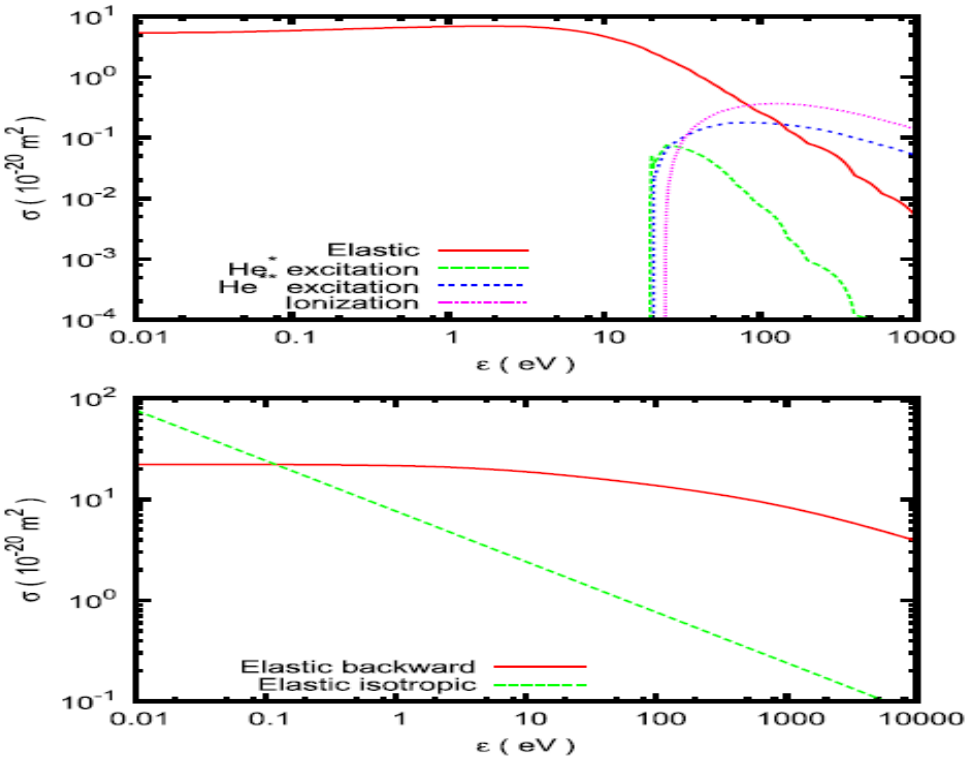

Figure 4.1. Electron and ion cross-sections taken from [38].

For all the cases, distance between the electrodes is 6.7 cm and neutral temperature is 300 K. Sinusoidal potential is applied from one electrode with certain amplitude with

frequency 13.56 MHz. Changing parameters are initial plasma density, neutral density, time step size and number of grids.

Table 4.1. Parameters taken from [38].

Case	V(V)	$N_0(10^{14}m^{-3})$	$N(10^{20}m^{-3})$	Δx (m)	Δt (s)	N_{ppc}
I	450	2.56	9.64	L/128	$(400f)^{-1}$	512
II	200	5.12	32.1	L/256	$(800f)^{-1}$	256
III	150	5.12	96.4	L/512	$(1600f)^{-1}$	128
IV	120	3.84	321	L/512	$(3200f)^{-1}$	64

In all the figures, continuous lines are present study results. As neutral density and pressure increases from case 1 to 4, power density profiles of both electrons and ions get closer to the sheath region. Good agreement is obtained with the benchmark cases, maximum relative error for mean ion densities is obtained in case 4 as 0.044. This value is far less in other cases. Particle weights are calculated with given particle per cell parameter as

$$w = \frac{nV_{cell}}{N_{ppc}}, \tag{4.1}$$

where V_{cell} and N_{ppc} are the volume of the cell and particle per cell respectively, n is the particle density. Volume is taken as length of the discharge and initial plasma density is used with the total super particle number.

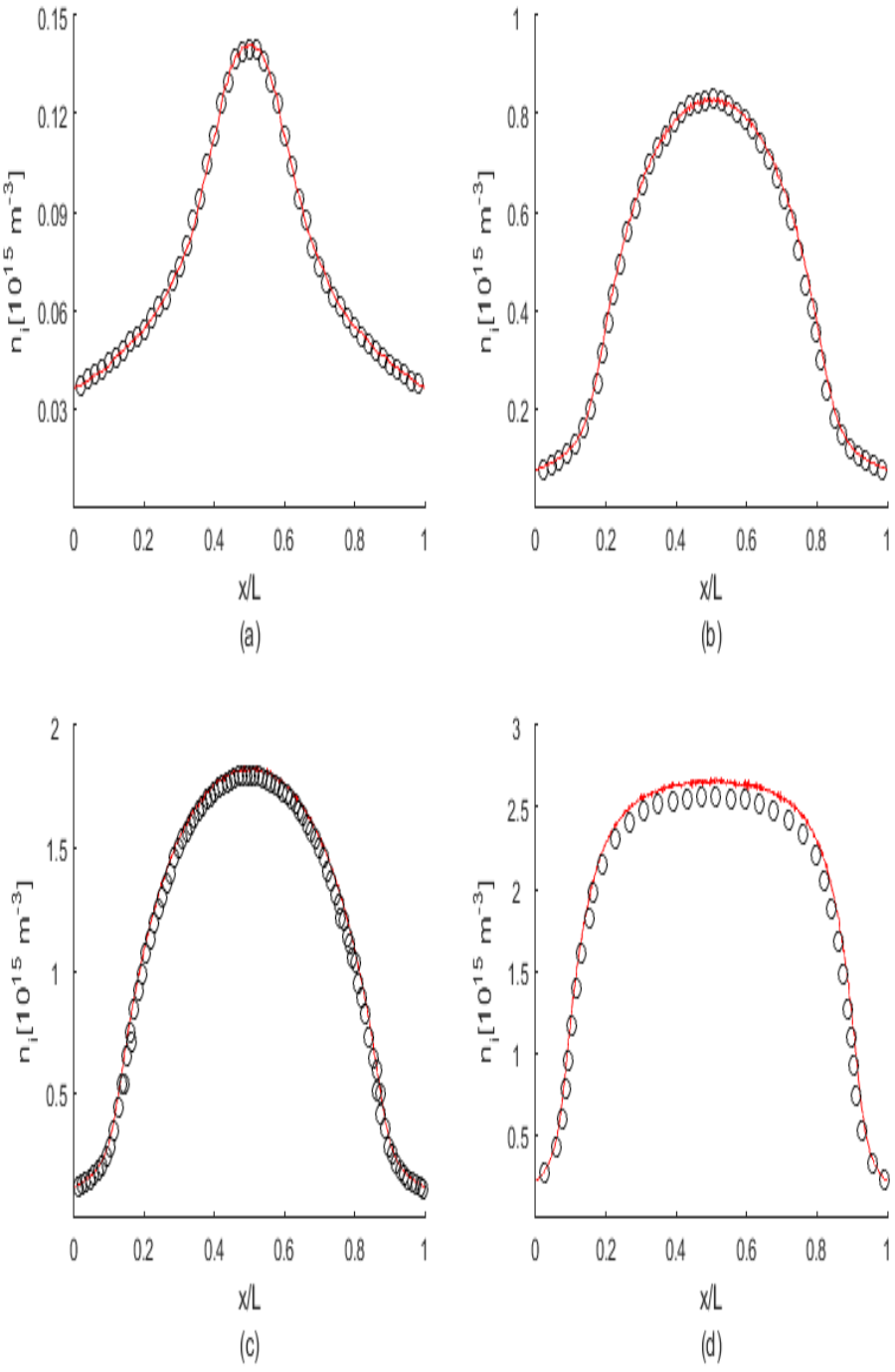

Figure 4.2. Comparison of mean ion densities with [38], continuous line is present study results. a) Case I, b) Case II, c) Case III, d) Case IV.

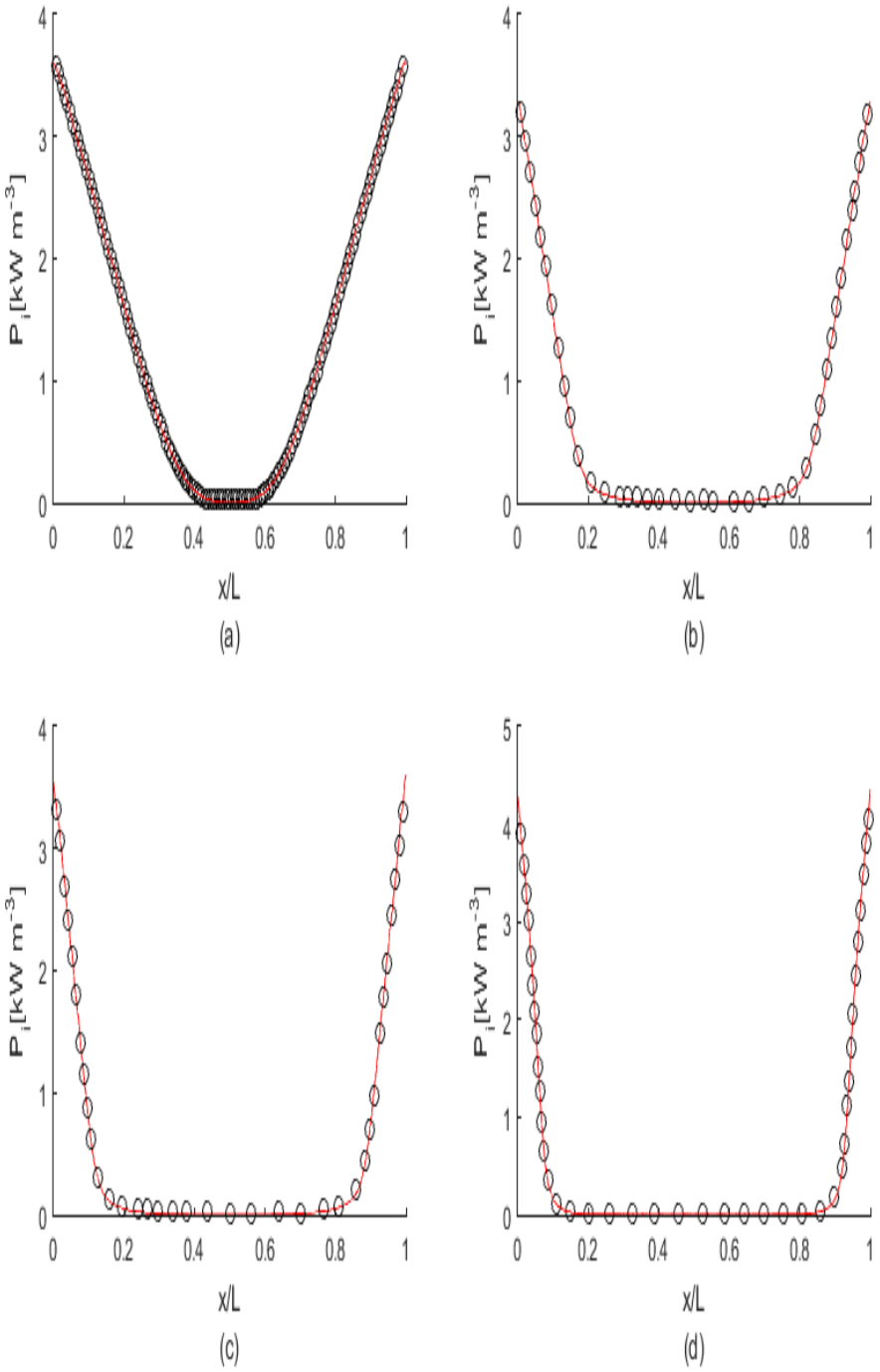

Figure 4.3. Comparison of ion heating rates with [38], continuous line is present study results. a) Case I, b) Case II, c) Case III, d) Case IV.

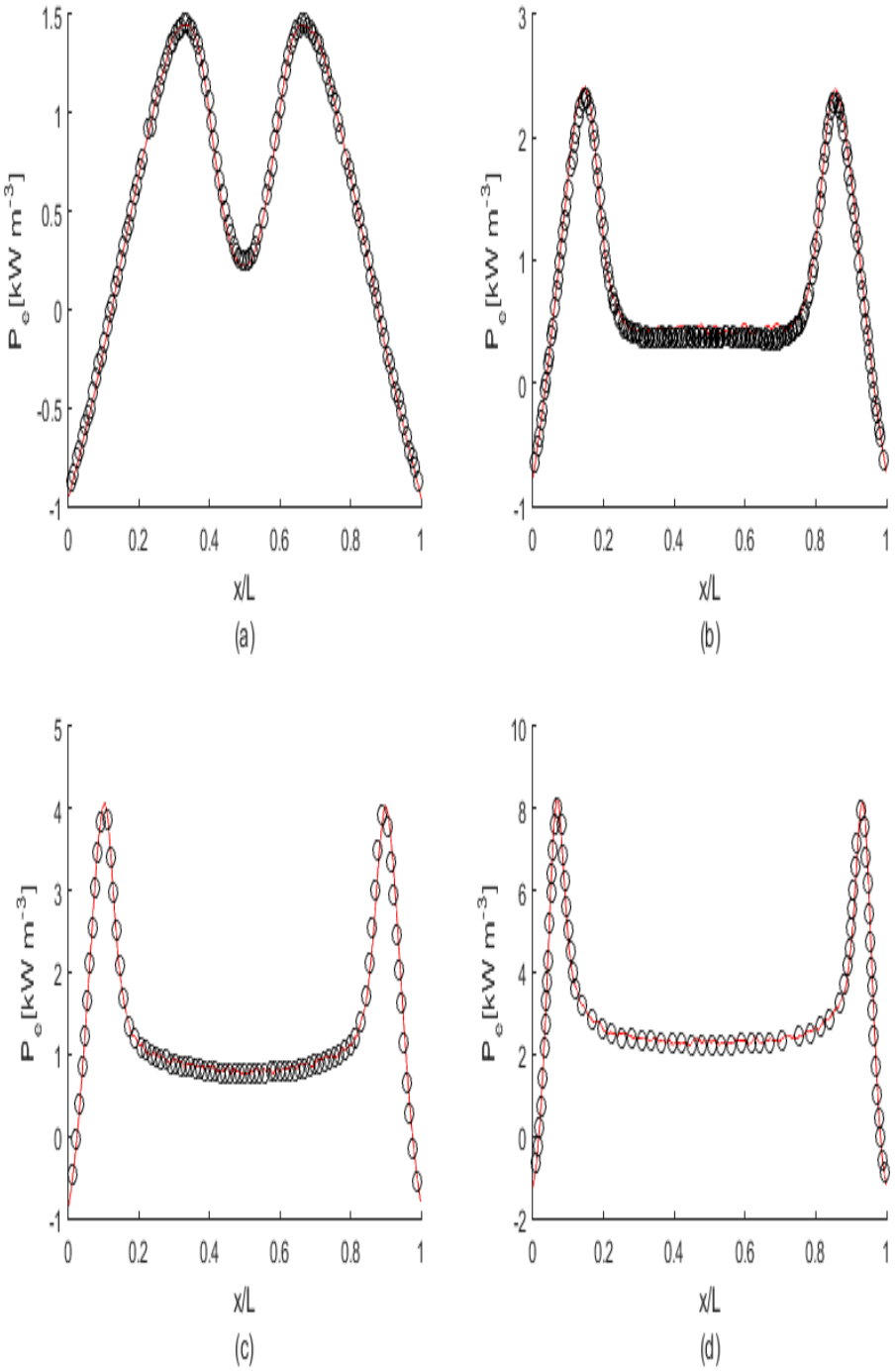

Figure 4.4. Comparison of electron heating rates with [38], continuous line is present study results. a) Case I, b) Case II, c) Case III, d) Case IV.

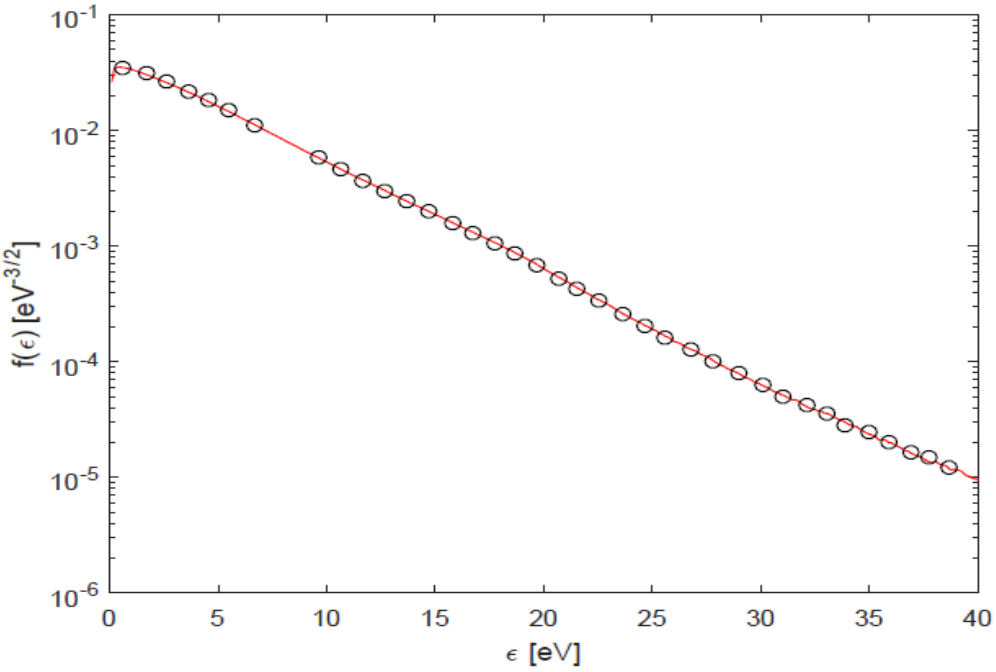

Figure 4.5. Electron energy distribution function case II. Comparison with [38]. Continuous line is present study result.

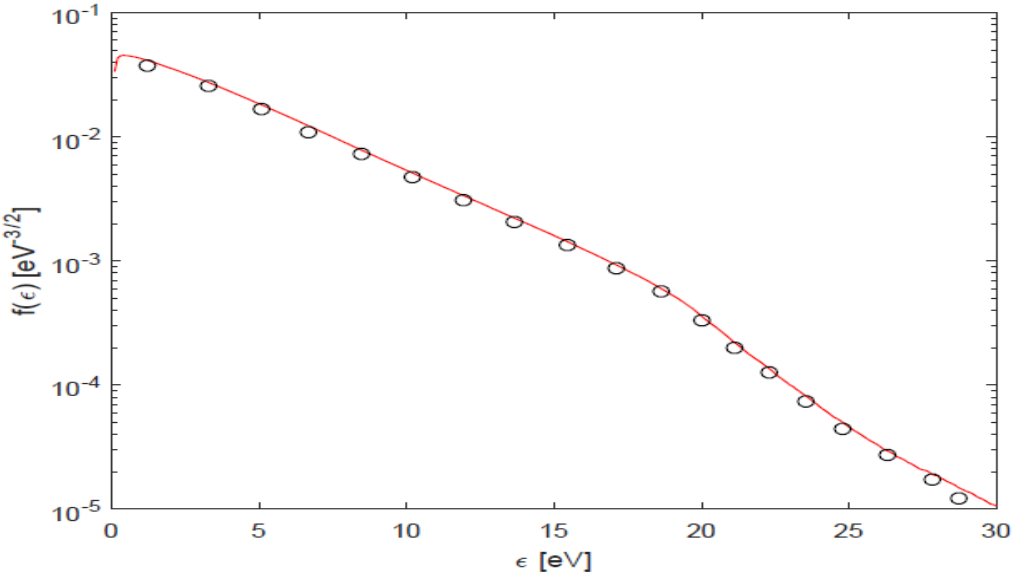

Figure 4.6. Electron energy distribution function case III. Comparison with [38]. Continuous line is present study result.

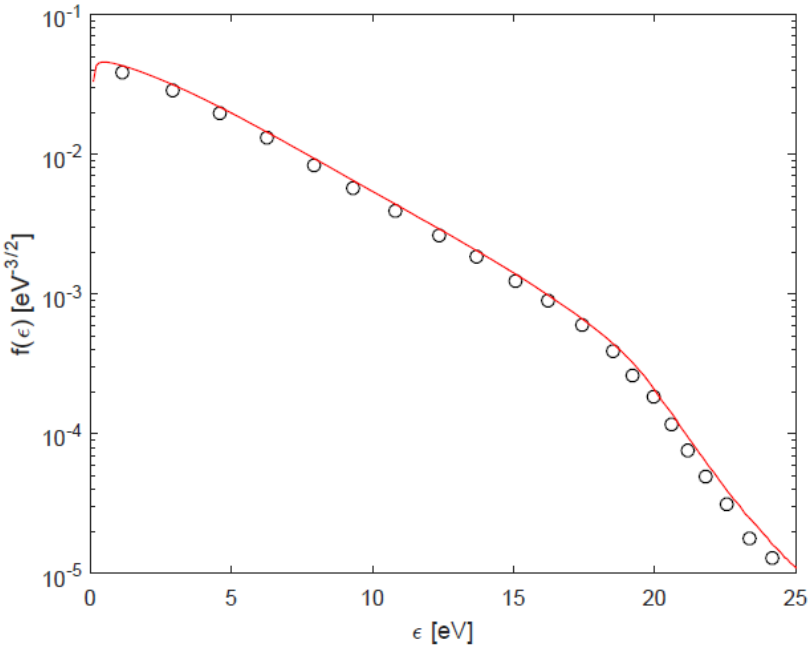

Figure 4.7. Electron energy distribution function case IV. Comparison with [38]. Continuous line is present study result.

Electron energy distribution function $f(\epsilon)$ is calculated by counting number of particles in the interval $(\epsilon, \epsilon + d\epsilon)$ [39] and it is normalized as

$$\int_0^\infty \sqrt{\epsilon}\, f(\epsilon) d\epsilon = 1 \tag{4.2}$$

4.2. 3D3V Electron Swarm in Argon

Parameters are taken from and results are compared with [32]. 500000 electrons from cathode are tracked until they are absorbed by the boundaries.

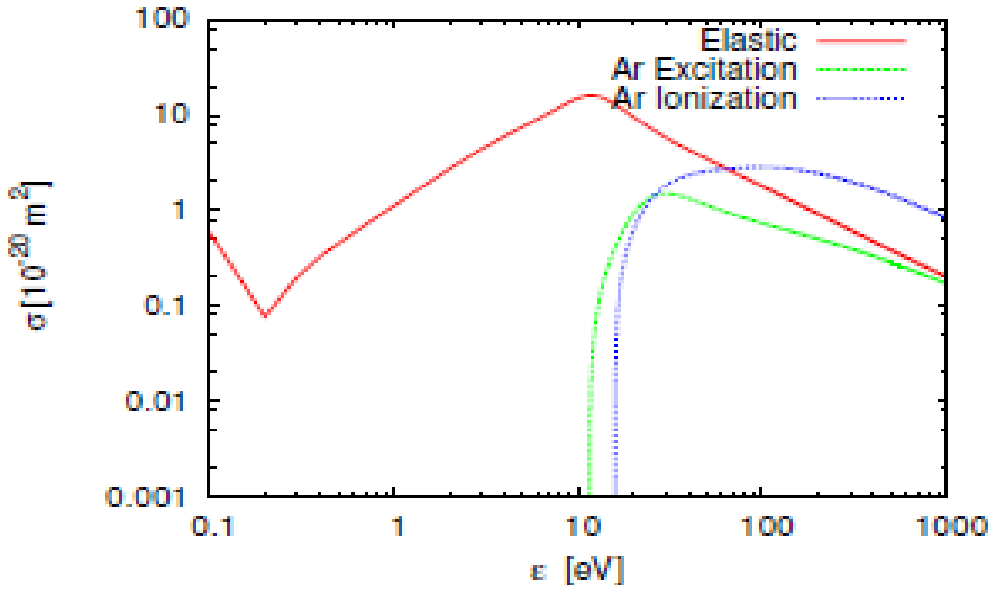

Figure 4.8. Electron-neutral cross sections for argon taken from [40].

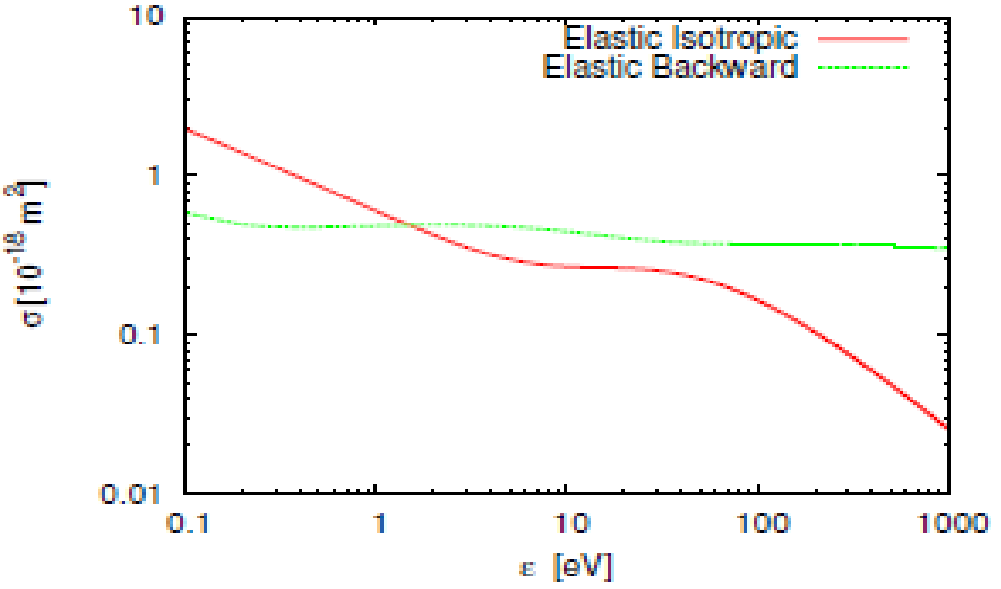

Figure 4.9. Ion-neutral cross sections for argon taken from [41].

Constant reduced electric field (E/n) is taken as 500 Td. Mean energy and drift velocity of electrons, ionization coefficient (first Townsend coefficient) are calculated. Ionization coefficient (α) is calculated as given [32] by

$$\alpha = \frac{d\phi_e(x)}{\phi_e(x)dx}, \tag{4.3}$$

where ϕ_e is the electron flux. Electrode distance and neutral temperature are 1 cm and 300 K respectively. Only absorption occurs at the boundaries. Near the cathode, system is not in equilibrium, mean electron energy increases. After electrons reach enough energy for excitation and ionization, electron number is multiplied with the ionization. Through center of discharge, mean energy decreases and reach an equilibrium value. Near the anode, mean electron energy again increases with the drift velocity. As number of energetic electrons decreases, ionization coefficient is lower than equilibrium value near the anode.

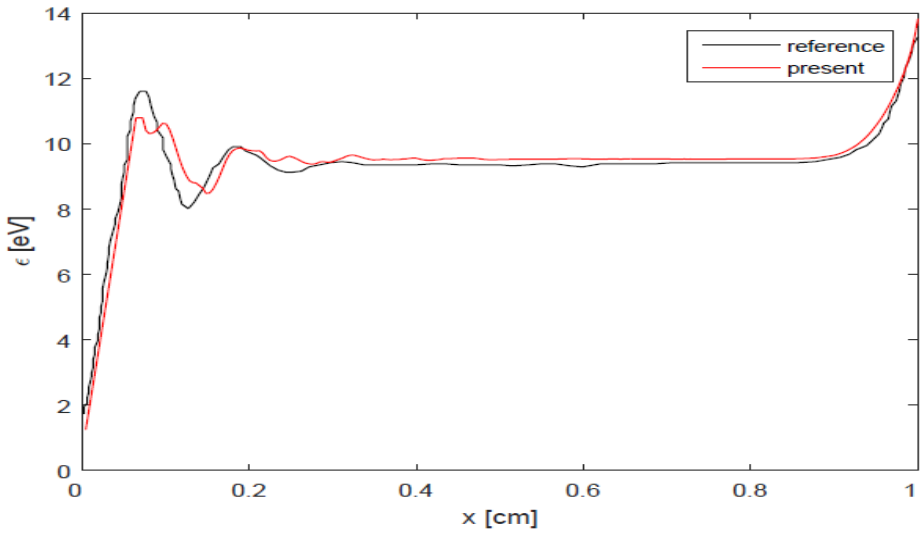

Figure 4.10. Mean energy, comparison with Ref. [32].

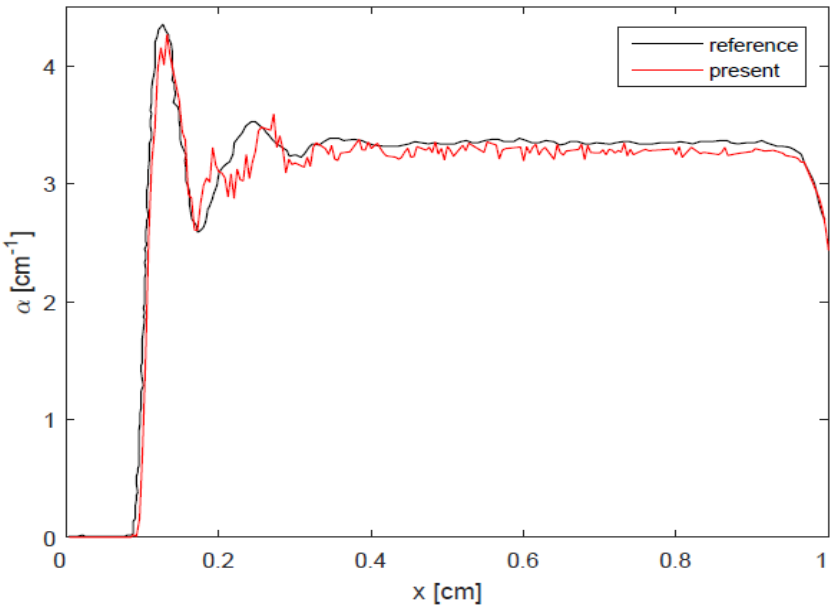

Figure 4.11. Ionization coefficient, comparison with Ref. [32].

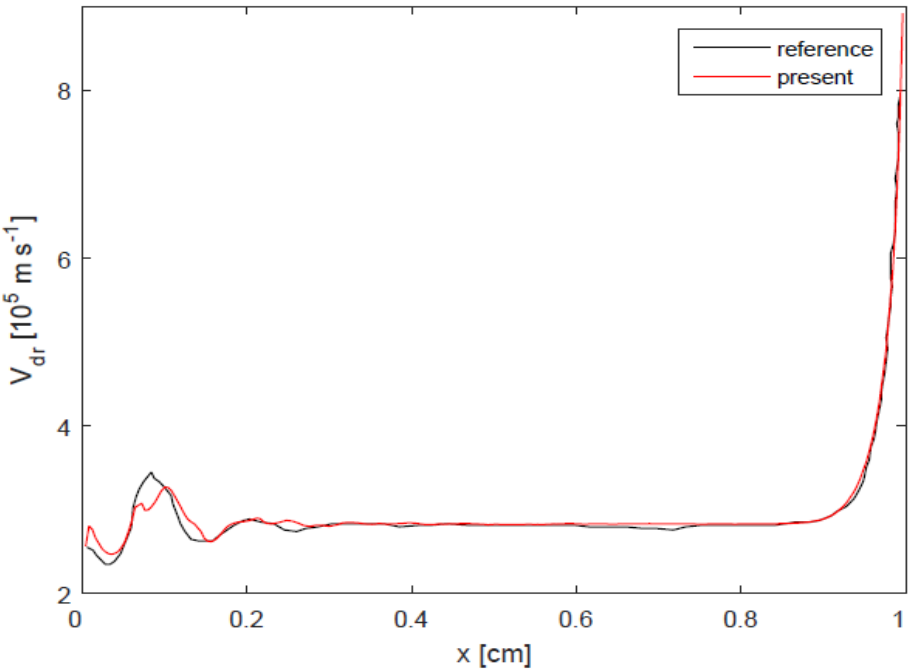

Figure 4.12. Drift velocity, comparison with Ref. [32].

4.3. RF Argon Discharge

Comparison is made with the parameters given by [42]. Boundary interactions are ignored. Two main type of discharge is distinguished by ionization source, namely α and γ types. For α type, main ionization source is primary electrons resulting from ionizing collisions. For γ type, ionization is mostly due to secondary electrons resulting from ion impact at the cathode. In this case, discharge is α type, secondary electron emission is ignored.

Table 4.2. Comparison parameters RF Argon discharge.

Parameter	Value
Gas type	Argon
Neutral pressure (p)	50 mTorr
Neutral temperature (T)	350 K
Potential (V)	350 V
Electrode distance (L)	2 cm
Frequency (f)	13.56 MHz
Grid size (Δx)	L/600
Weight	$2.5x10^8$

Maximum relative error for particle densities is calculated using difference between maximum values by

$$\varepsilon_{\text{rel}} = \frac{max|n_{ref} - n|}{max|n_{ref}|} \tag{4.4}$$

For mean electron density ε_{rel} is calculated to be about 0.029. Quantitative comparison could not be done for spatio-temporal plots. Accuracy is in the limit of 80-90%.

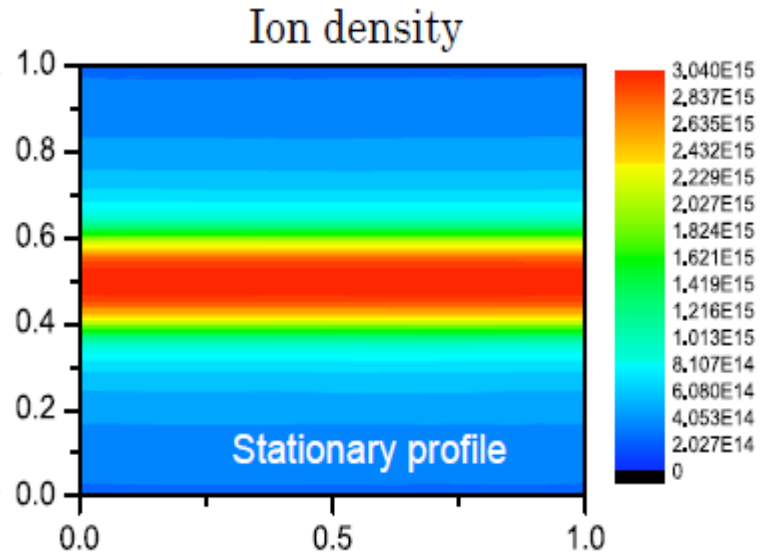

(a)

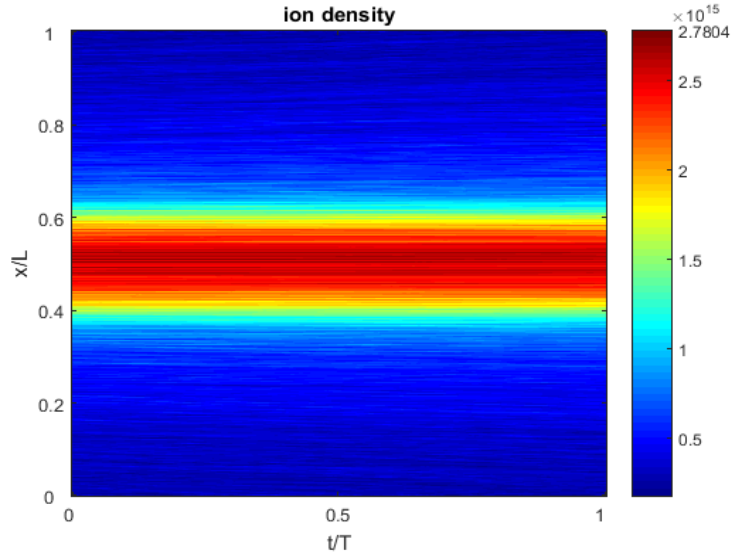

(b)

Figure 4.13. Ion density (10^{15} m^{-3}) for Argon, p=50mTorr, V=350 V, L= 2 cm. a) Result of Ref. [42], b) Present study result.

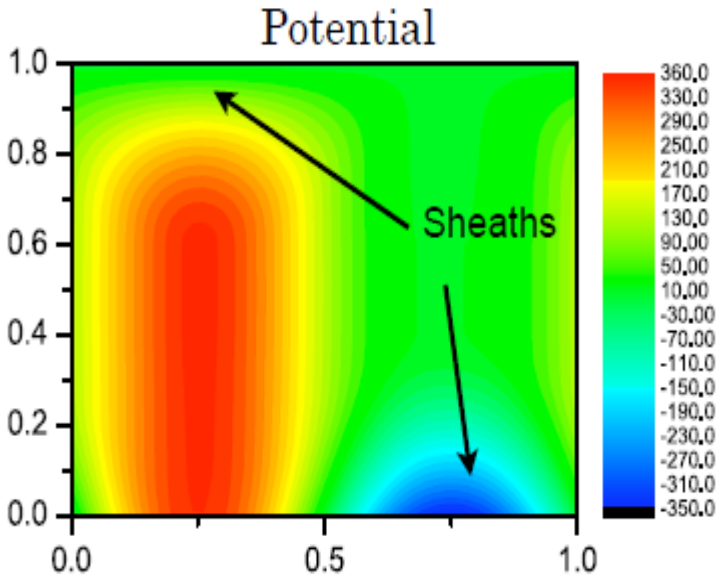

(a)

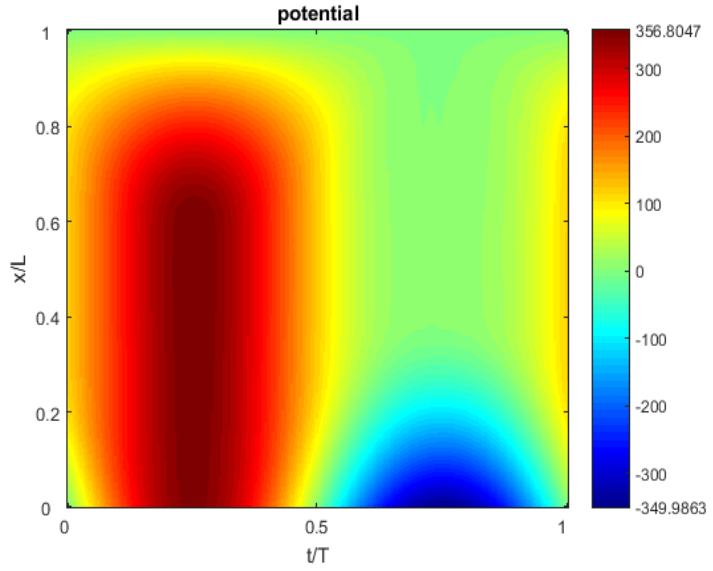

(b)

Figure 4.14. Potential (V) for Argon, p=50mTorr, V=350 V, L= 2 cm. a) Result of Ref. [42], b) Present study result.

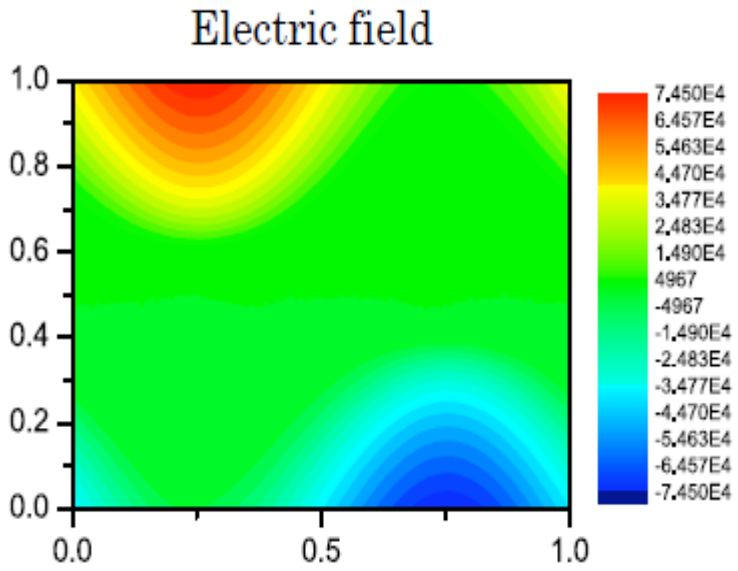

(a)

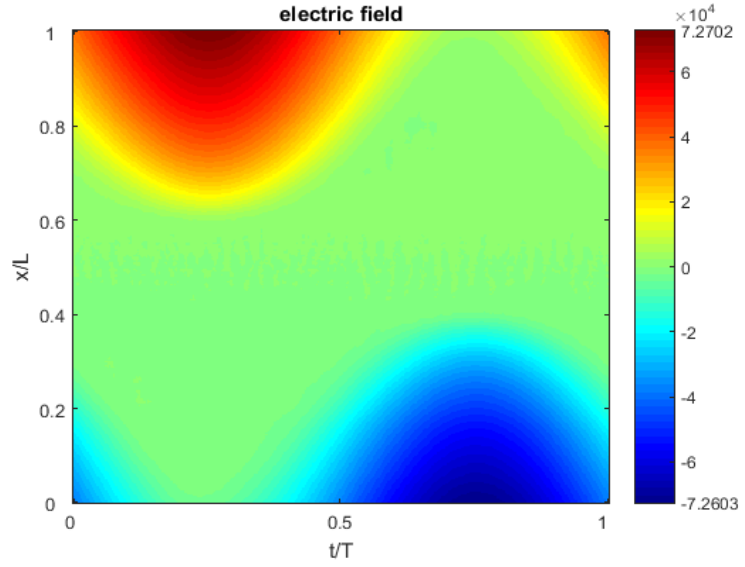

(b)

Figure 4.15. Electric field (10^4 V/m) for Argon, p=50mTorr, V=350 V, L= 2 cm. a) Result of Ref. [42], b) Present study result.

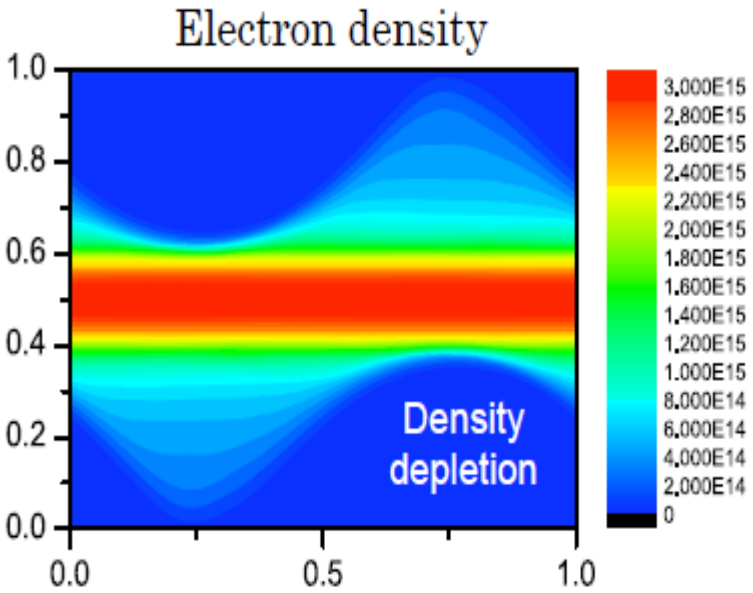

(a)

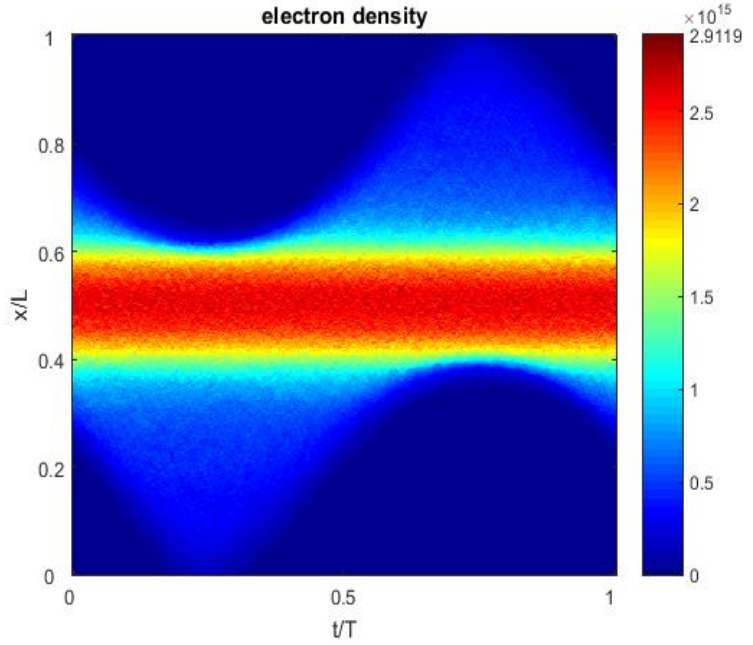

(b)

Figure 4.16. Electron density (10^{15} m^{-3}) for Argon, p=50mTorr, V=350 V, L= 2 cm. a) Result of Ref. [42], b) Present study result.

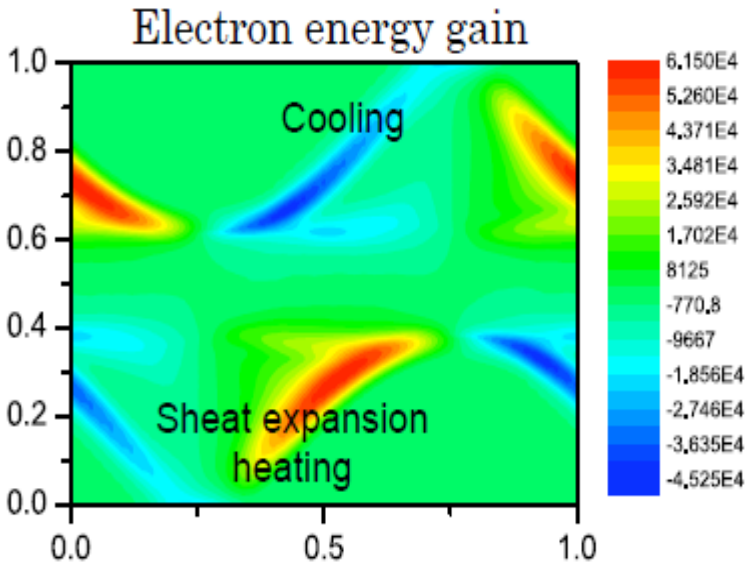

(a)

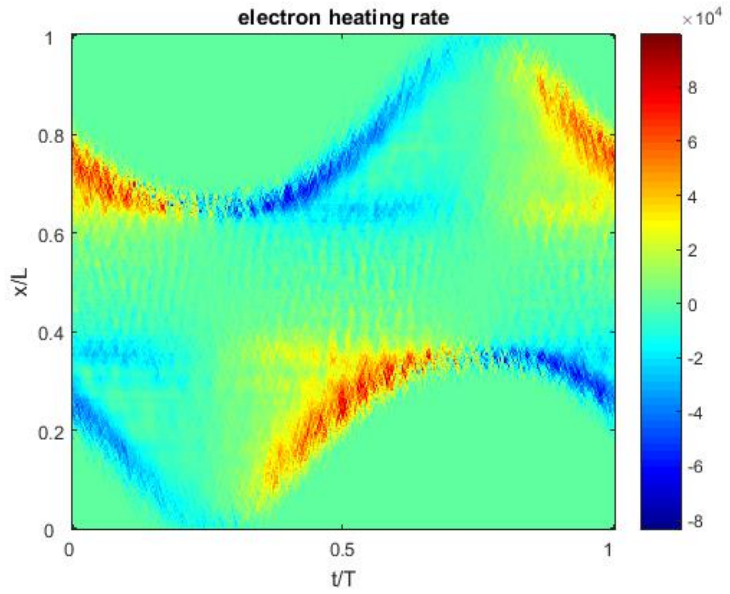

(b)

Figure 4.17. Electron heating rate (Wm^{-3}) for Argon, p=50mTorr, V= 350 V, L=2cm a) Result of Ref. [42], b) Present study result.

4.4. Effects of Electron Reflection at The Boundaries

In this case, electron reflection at the boundaries is included and results are compared with the complete absorption for the RF helium discharge. Electrons are reflected without energy loss. Main ionization source is electron impact ionization of primary electrons for relatively low pressure of 10 Pa. Reflection coefficient is taken as 0.2. Secondary electron emission due to ion impact is not included.

Table 4.3. Comparison parameters for reflection at the boundaries for Helium.

Parameter	Value
Gas type	Helium
Neutral pressure (p)	10 Pa
Neutral temperature (T)	300 K
Potential (V)	240 V
Electrode distance (L)	6.7 cm
Frequency (f)	13.56 MHz
Time step size (Δt)	$(3200f)^{-1}$
Grid size (Δx)	L/512
Reflection coefficient (r)	0.2
Weight	7.8515×10^{8}

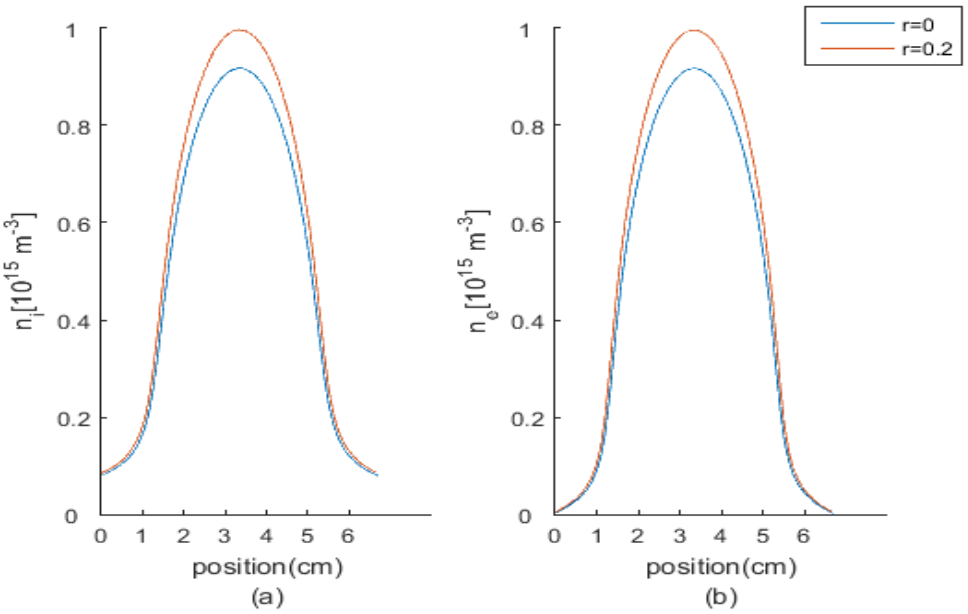

Figure 4.18. Comparison of particle densities with reflection for helium discharge a) ion density, b) electron density.

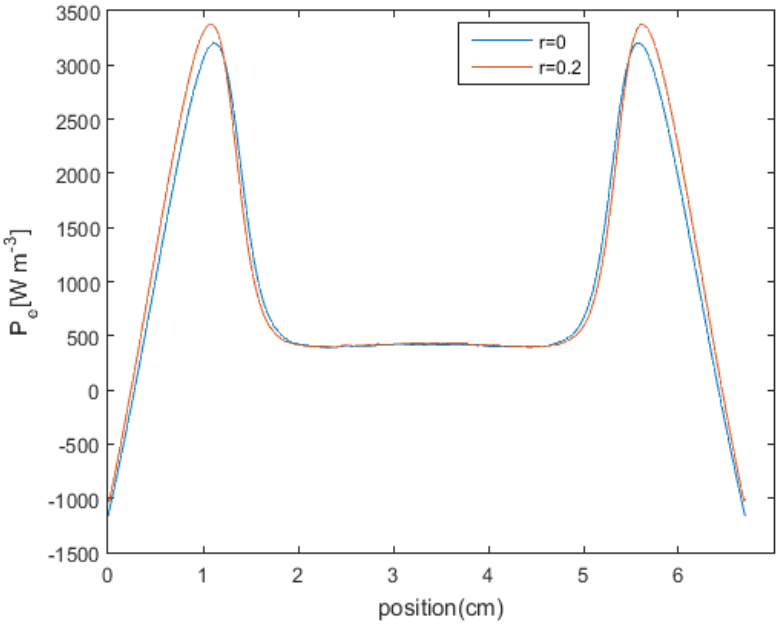

Figure 4.19. Comparison of electron heating rate with reflection for helium discharge.

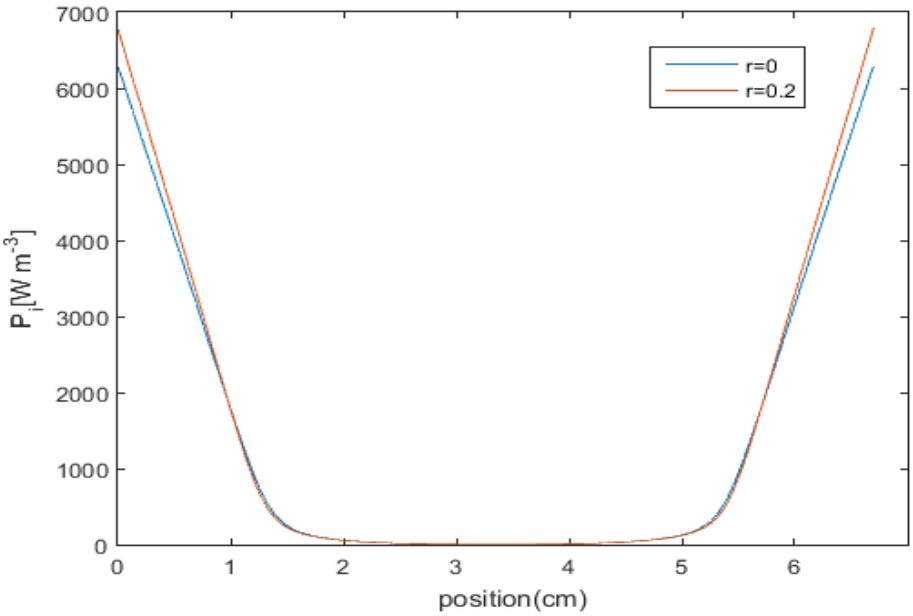

Figure 4.20. Comparison of ion heating rate with reflection for helium discharge.

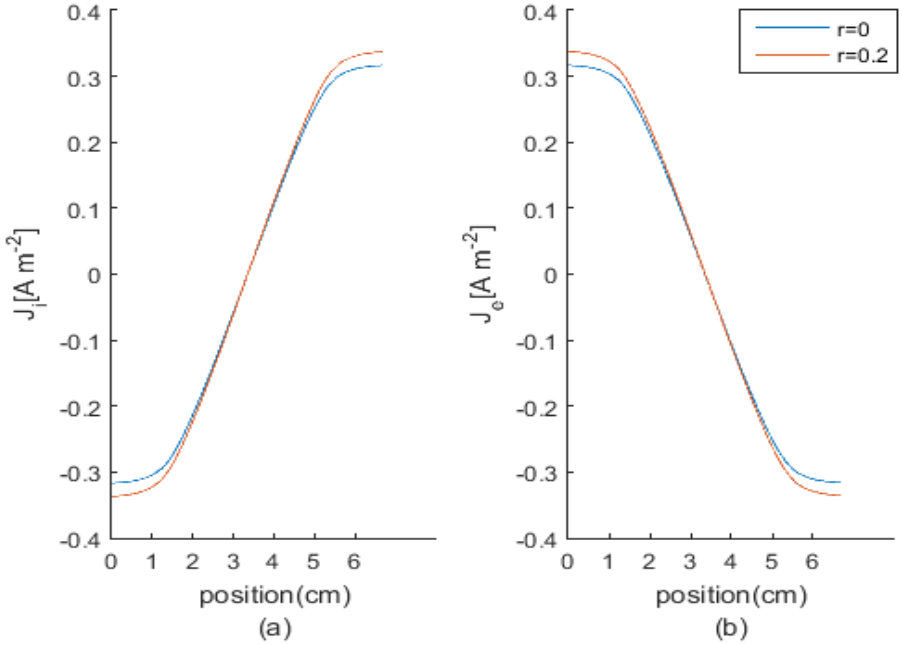

Figure 4.21. Comparison of current densities with reflection for Helium discharge a) ion current density, b) electron current density.

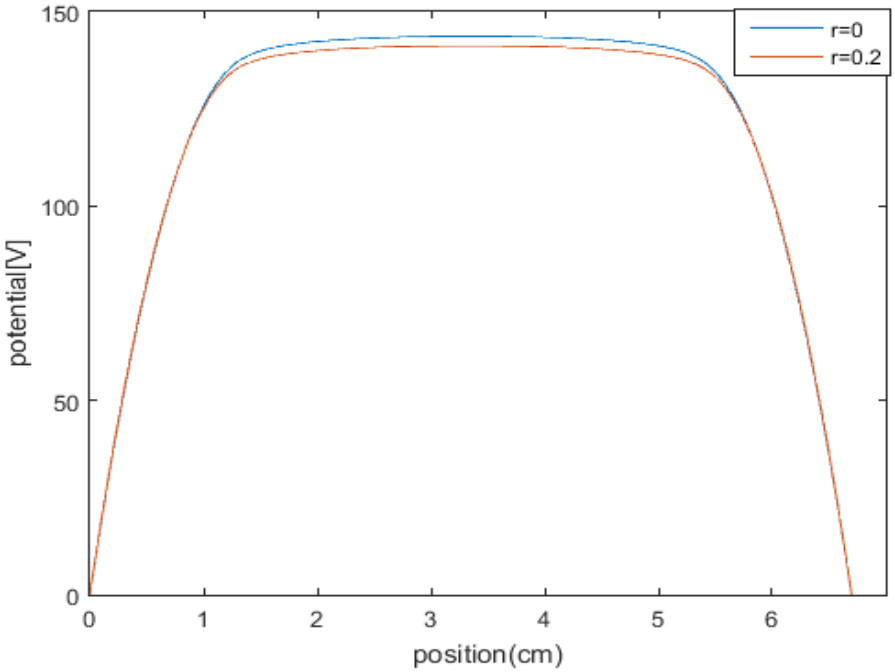

Figure 4.22. Comparison of potential with reflection for Helium discharge.

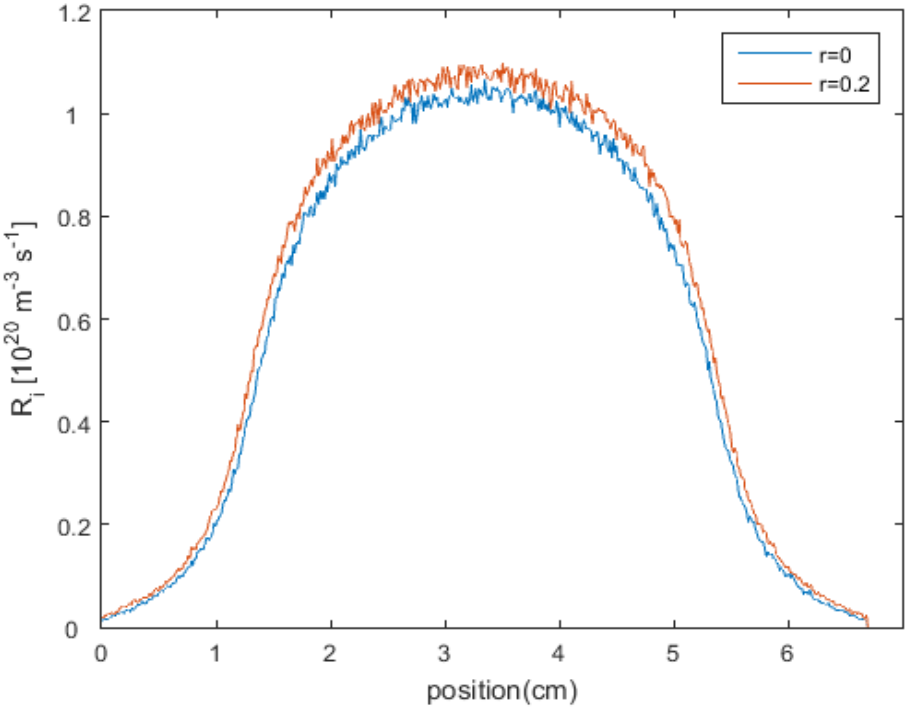

Figure 4.23. Comparison of ionization rate with reflection for Helium discharge.

For comparison, simulation was performed for 13000 RF cycles (~1 ms) and results are averaged over 5000 RF cycle (~0.3 ms) which corresponds to 16 x 10^6 time steps. Ionization rate is highest at the center of the discharge. Ionization rate, particle densities, heating rates and current densities are increased by reflection of electrons. Potential in the center of the discharge is slightly reduced by reflection.

4.5. RF Argon Discharge Analysis

Detailed results of the code for Argon discharge is given. Secondary electron emission due to impact of positive ions is included with the coefficient of 0.2. For ions, sub-cycling is used with coefficient of 5. Results are averaged over 20 RF cycles except for instances of one RF period.

Table 4.4. Parameters for RF Argon discharge.

Parameter	Value
Gas type	Argon
Neutral pressure (p)	40 Pa
Neutral temperature (T)	300 K
Potential (V)	200 V
Electrode distance (L)	2 cm
Frequency (f)	13.56 MHz
Grid size (Δx)	L/512
Secondary electron yield (γ)	0.2
Reflection coefficient (r)	0.2
Ion sub-cycling coefficient	5
Weight	7.8515×10^8

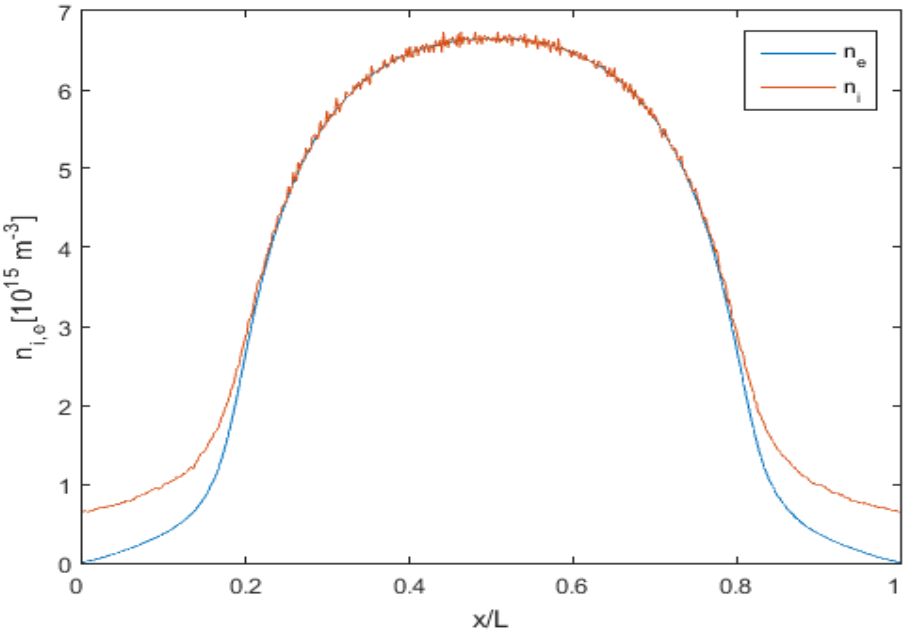

Figure 4.24. Electron and ion densities for argon.

Ion density is higher than electron density in the sheath region as they are accelerated towards electrodes while electrons are accelerated towards bulk with strong electric field in the sheaths.

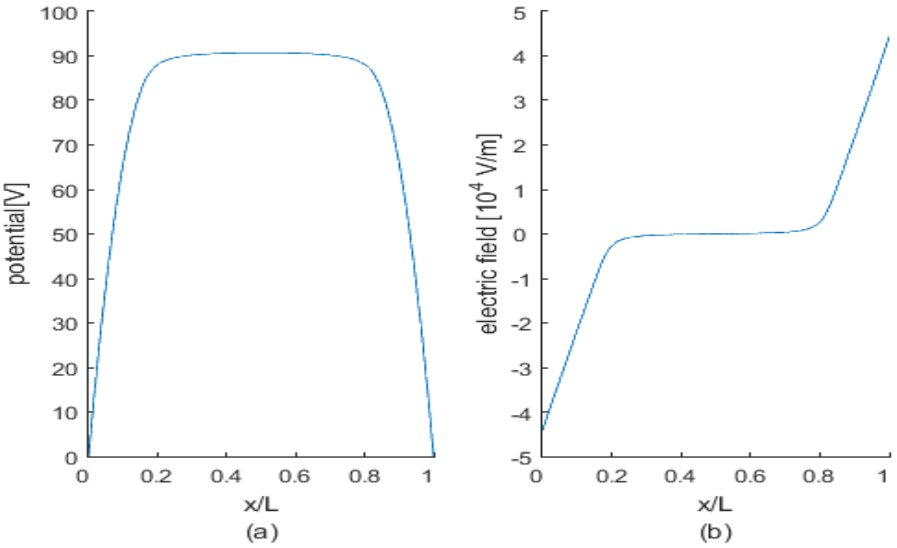

Figure 4.25. a) Potential for argon, b) Electric field for argon.

Electric field at the bulk region is close to zero, while it changes over sheath regions.

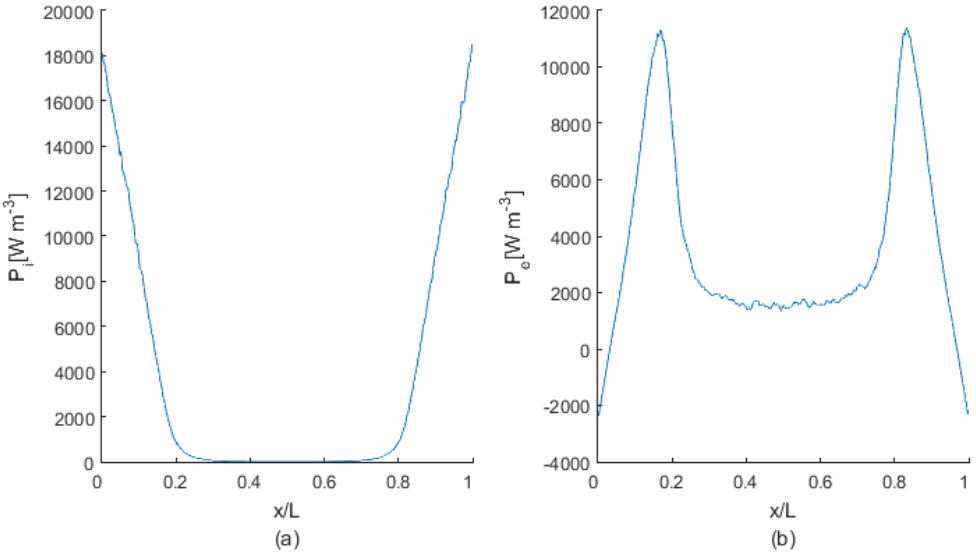

Figure 4.26. a) Ion heating rate for argon, b) Electron heating rate for argon.

Energy gain of electrons increase towards the sheath edges, while it reduces an equilibrium value in the center of the discharge. For ions, there is strong energy gain in sheath regions.

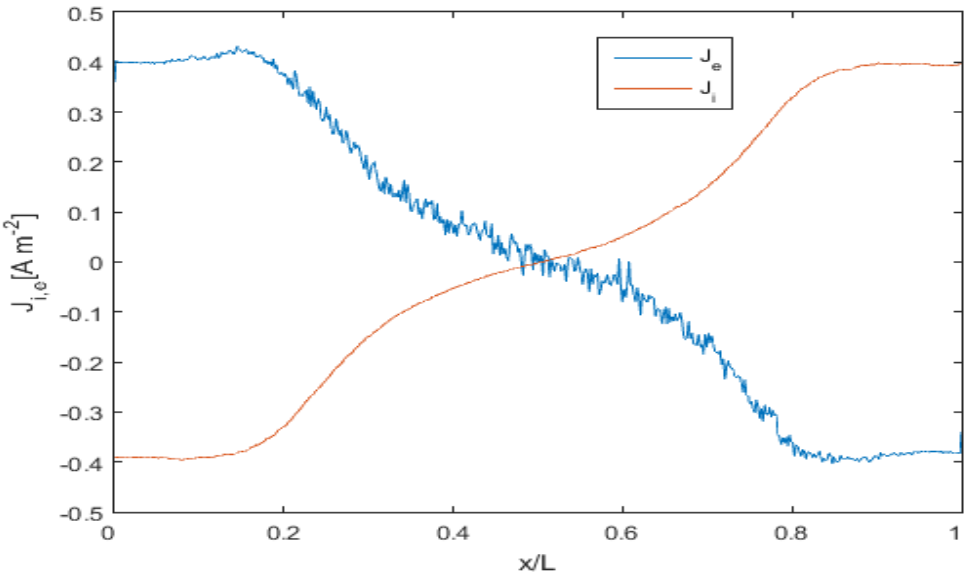

Figure 4.27. Electron and ion current densities (J_e, J_i) for argon.

Current densities are calculated by multiplying charge densities with average velocities of particles on grid points as

$$J_{e,i} = n_{e,i} < v_{x\,e,i} > q_{e,i} \tag{4.4}$$

where $n_{e,i}$, $<v_x>$ and q are particle densities, average velocity on grid points in the x-direction and elementary charge respectively.

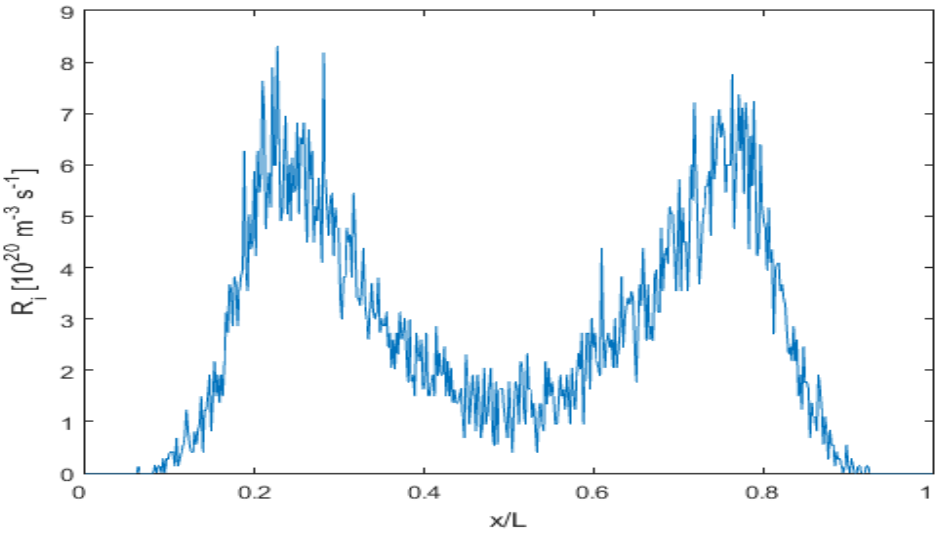

Figure 4.28. Ionization rate for argon.

Ionization rate is calculated by counting ionizing collisions in every time step and seen to be greatest at the sheath edges with the effect of the accelerated energetic electrons. It reduces through the center of the discharge.

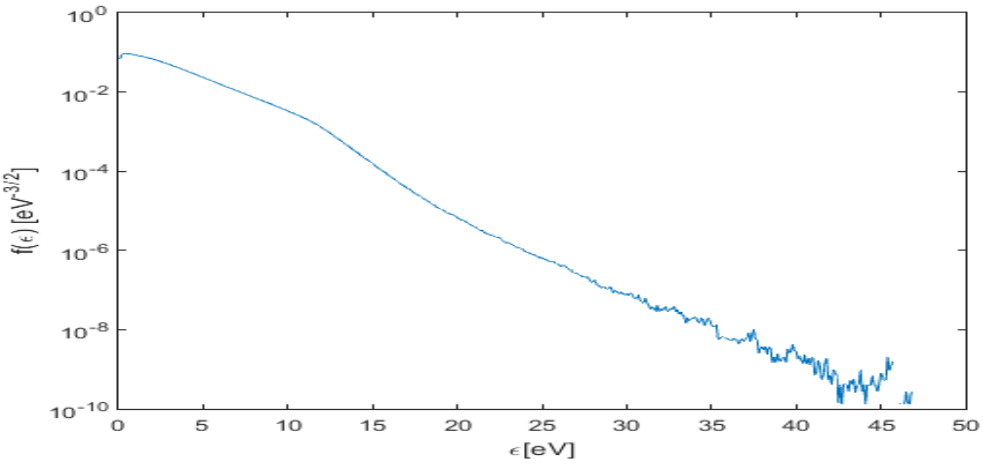

Figure 4.29. Electron energy distribution function for argon.

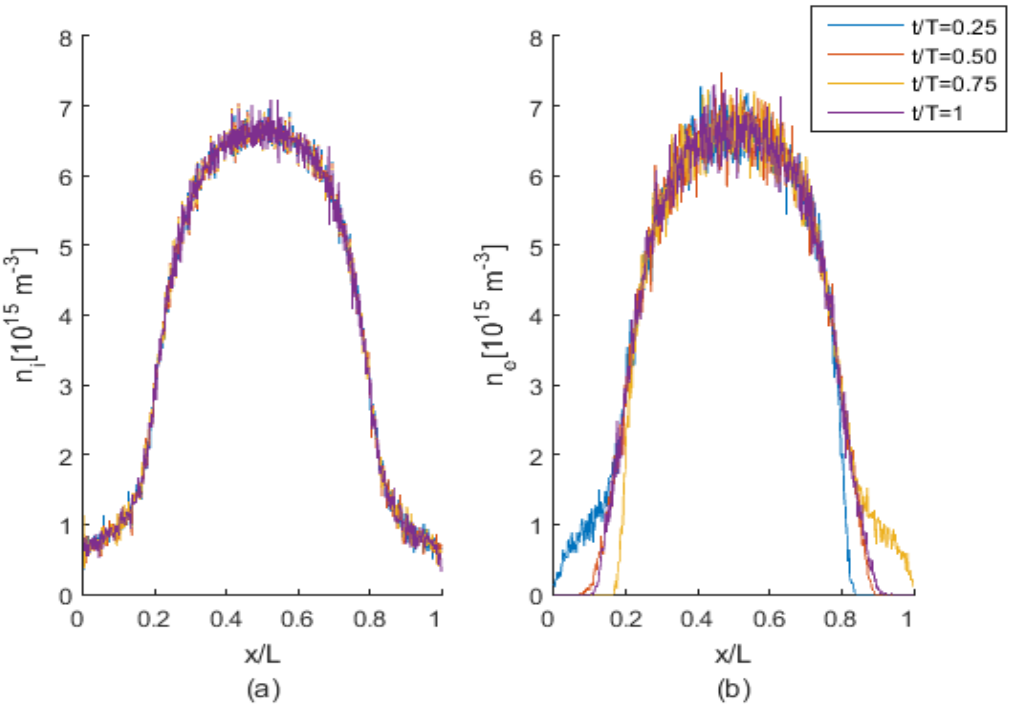

Figure 4.30. Particle densities at instances of RF period for argon a) Ion, b) Electron.

Symmetrical results for particle densities are observed for given instances of RF period. Ion density remains to be constant through the discharge while electron density changes periodically in the sheath region.

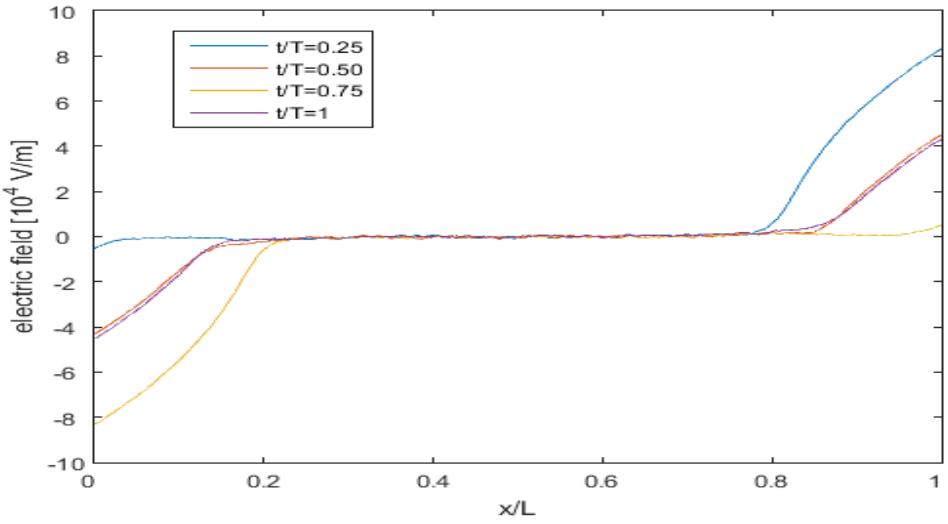

Figure 4.31. Electric field at instances of RF period for argon.

Electric field also gives periodic results at given instances of RF period as expected.

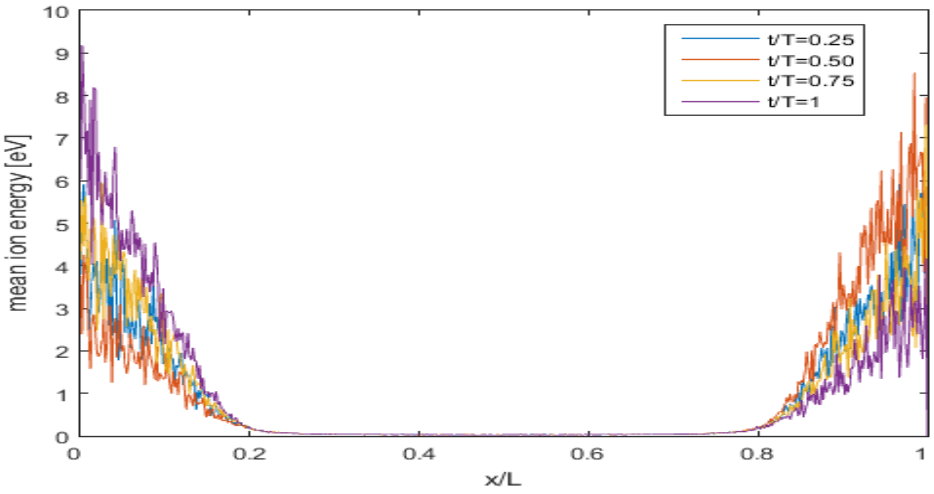

Figure 4.32. Mean ion energies at instances of RF period for argon.

Mean ion energies increase in the sheath region towards the electrodes and remain constant and very low in the bulk. They also show periodic results at instances of RF period. It is an important parameter for surface applications in RF discharges.

In general, symmetrical results for particle densities, electric field and mean ion energies for instances of RF period ($wt/2\pi$) are observed. Results are obtained after 5000 RF cycles.

CHAPTER 5

CONCLUSION

In this study, 1d3v kinetic code for discharge plasma simulations was developed and validated by using Particle in cell/Monte Carlo Collision (PIC/MCC) method. The model is three-dimensional in velocity space. The code was parallelized using MPI and written in Fortran 90 language. Null-collision method was used for particle collisions. Validation was done by benchmarks for capacitively coupled Helium discharges from the literature and the code is applied for 3d3v model of electron swarm in Argon. Boundary effect of reflection of electrons was compared for RF Helium discharge resulting overall increase in particle energy gain, current densities and ionization rate. Results of the code were compared with the presented results for RF Argon discharge.

For future works, the model can be developed with advanced management of particle weights [43] which is an important parameter for accuracy and performance of particle codes. Model can be improved with more efficient parallelization, higher performance can be achieved for simulation of more realistic systems and advanced geometries.

REFERENCES

[1] M.A. Lieberman and A.J. Lichtenberg, *Discharges and Materials Processing Principles of Plasma Discharges and Materials*. *Wiley-Interscience*, 2005.

[2] M. Capitelli and C. Gorse, *Plasma Technology*. *Springer US*, Boston, MA, 1992.

[3] S. Eliezer and Y. Eliezer, *The Fourth State of Matter An Introduction to Plasma Science*. *IOP Publishing Ltd*, 2001.

[4] P.K. Chu and X. Lu, Eds., *Low Temperature Plasma Technology*. *CRC Press*, 2013.

[5] D. Tskhakaya, K. Matyash, R. Schneider, and F. Taccogna, "The particle-in-cell method.," *Contributions to Plasma Physics*. vol. 47, no. 8–9, pp. 563–594, 2007.

[6] G.J.M. Hagelaar and L.C. Pitchford, "Solving the Boltzmann equation to obtain electron transport coefficients and rate coefficients for fluid models.," *Plasma Sources Science and Technology*. vol. 14, no. 4, pp. 722–733, 2005.

[7] Z. Donkó, "Hybrid model of a rectangular hollow cathode discharge.," *Physical Review E - Statistical Physics, Plasmas, Fluids, and Related Interdisciplinary Topics*. vol. 57, no. 6, pp. 7126–7137, 1998.

[8] R.K. Marcus, *Glow Discharge Plasmas in Analytical Spectroscopy*. *John Wiley & Sons, Ltd*, Chichester, UK, 2002.

[9] A.M. Howatson, *Introduction to gas discharges*. *Pergamon Press Ltd*, 1976.

[10] Y.P. Raizer, *Gas Discharge Physics*. *Springer-Verlag*, Berlin, 1991.

[11] A. Fridman and L. A. Kennedy, *Plasma Physics and Engineering*. *CRC Press*, 2011.

[12] F.F. Chen, *Introduction to Plasma Physics and Controlled Fusion*. *Springer*, 2016.

[13] J. Meichsner, M. Schmidt, R. Schneider, and H.-E. Wagner, *Nonthermal Plasma Chemistry and Physics*. *CRC Press*, 2012.

[14] T. Makabe and Z.L. Petrovic, *Plasma Electronics, Second Edition: Applications in Microelectronic Device Fabrication*. *CRC Press*, 2015.

[15] J.A. Bittencourt, *Fundamentals of plasma physics*. *Springer*, 2004.

[16] S. Longo, “Monte Carlo simulation of charged species kinetics in weakly ionized gases.,” *Plasma Sources Science and Technology*. vol. 15, no. 4, pp. S181–S188, 2006.

[17] G. Lapenta, “Kinetic Plasma Simulation: Particle In Cell Method.,” *XII Carolus Magnus Summer School on Plasma and Fusion Energy Physics*. pp. 76–85, 2015.

[18] C.K. Birdsall and A.B. Langdon, *Plasma Physics via Computer Simulation*. *IOP Publishing Ltd*, 1991.

[19] C.K. Birdsall, “Particle-in-cell charged-particle simulations, plus Monte Carlo collisions with neutral atoms, PIC-MCC.,” *IEEE Transactions on Plasma Science*. vol. 19, no. 2, pp. 65–85, 1991.

[20] A. Sun, M.M. Becker, and D. Loffhagen, “PIC/MCC simulation of capacitively coupled discharges: Effect of particle management and integration.,” *Computer Physics Communications*. vol. 206, pp. 35–44, 2016.

[21] N. Hanzlikova and M.M. Turner, “Leap frog integrator modifications in highly collisional particle-in-cell codes.,” *Journal of Computational Physics*. vol. 268, pp. 355–362, 2014.

[22] W. Brok, *Modelling of transient phenomena in gas discharges.*, 2005.

[23] S. Ross, *A First Course in Probability*. *Pearson*, 2010.

[24] A. Haghighat, *Monte Carlo Methods for Particle Transport*. *CRC Press*, 2015.

[25] G.A. Bird, *Molecular gas dynamics and the direct simulation of gas flows*. *Clarendon Press*, 1994.

[26] R.W. Hockney and J.W. Eastwood, *Computer Simulation Using Particles*. *IOP Publishing Ltd*, 1988.

[27] V. Vahedi and M. Surendra, “A Monte Carlo collision model for the particle-in-cell method: applications to argon and oxygen discharges.,” *Computer Physics Communications*. vol. 87, no. 1–2, pp. 179–198, 1995.

[28] K. Nanbu, “Probability theory of electron-molecule, ion-molecule, molecule-molecule, and Coulomb collisions for particle modeling of materials processing plasmas and gases.,” *IEEE Transactions on Plasma Science*. vol. 28, no. 3, pp. 971–990, 2000.

[29] J.P. Verboncoeur, “Particle simulation of plasmas: Review and advances.,” *Plasma Physics and Controlled Fusion*. vol. 47, no. 5 A, p. 2005.

[30] Y. Itikawa, *Molecular Processes in Plasmas*. *Springer*, 2007.

[31] F. Taccogna, “Monte Carlo Collision method for low temperature plasma simulation.,” *Journal of Plasma Physics*. vol. 81, no. 1, p. 2015.

[32] Z. Donkó, “Particle simulation methods for studies of low-pressure plasma sources.,” *Plasma Sources Science and Technology*. vol. 20, no. 2, p. 2011.

[33] L. Savino, “Monte Carlo models of electron and ion transport in non-equilibrium plasmas.,” *Plasma Sources Science and Technology*. vol. 9, no. 4, p. 468, 2000.

[34] A.C. Elster, “Parallelization Issues and Particle-in-Cell Codes,” (1994).

[35] G.E. Karniadakis and R.M.K. Ii, *Parallel Scientific Computing in C ++ and MPI A seamless approach to parallel algorithms and their implementation*. *Cambridge University Press*, 2003.

[36] E. Kawamura, C.K. Birdsall, and V. Vahedi, “Physical and numerical methods of speeding up particle codes and paralleling as applied to RF discharges.,” *Plasma Sources Science and Technology*. vol. 9, no. 3, pp. 413–428, 2000.

[37] Z. Donkó, J. Schulze, U. Czarnetzki, et al., “Fundamental investigations of capacitive radio frequency plasmas: Simulations and experiments.,” *Plasma Physics and Controlled Fusion*. vol. 54, no. 12, p. 2012.

[38] M.M. Turner, A. Derzsi, Z. Donkó, et al., “Simulation benchmarks for low-pressure plasmas: Capacitive discharges.,” *Physics of Plasmas*. vol. 20, no. 1, p. 2013.

[39] S. Longo and M. Capitelli, “A simple approach to treat anisotropic elastic collisions in Monte Carlo calculations of the electron energy distribution function in cold plasmas.,” *Plasma Chemistry and Plasma Processing*. vol. 14, no. 1, pp. 1–13, 1994.

[40] A. V. Phelps and Z.L. Petrović, “Cold-cathode discharges and breakdown in argon: surface and gas phase production of secondary electrons.,” *Plasma Sources Science and Technology*. vol. 8, no. 3, p. 1999.

[41] A. V. Phelps, “The application of scattering cross sections to ion flux models in discharge sheaths.,” *Journal of Applied Physics*. vol. 76, no. 2, pp. 747–753, 1994.

[42] Z. Donko, “Particle in Cell simulations of capacitive RF discharges.,” *Ruhr University Presentation*. p. 2010.

[43] A. Sun, M.M. Becker, and D. Loffhagen, “PIC/MCC simulation of capacitively coupled discharges in helium: Boundary effects.,” *Plasma Sources Science and Technology*. vol. 27, no. 5, p. 2018.